The Medial Offshore Record of Explosive Volcanism Along the Central to Eastern Aegean Volcanic Arc: 2. Tephra Ages and Volumes, Eruption Magnitudes and Marine Sedimentation Rate Variations

S. Kutterolf, A. Freundt, T. Druitt, J. Mcphie, P. Nomikou, K. Pank, J. C Schindlbeck-belo, T. H Hansteen, S. R Allen

Geochemistry, Geophysics, Geosystems®

AGU ADVANCING EARTH AND SPACE SCIENCE

RESEARCH ARTICLE
10.1029/2021GC010011

This article is a companion to Kutterolf, Freundt, Hansteen, et al. (2021), https://doi.org/10.1029/2021GC010010.

Key Points:

- Tephrochronology for the Aegean Arc eruptions
- Sedimentation rate variability in the Aegean Sea
- Eruptive volumes and masses for the major Aegean Arc eruptions

Supporting Information:

Supporting Information may be found in the online version of this article.

Correspondence to:

S. Kutterolf,
skutterolf@geomar.de

Citation:

Kutterolf, S., Freundt, A., Druitt, T. H., McPhie, J., Nomikou, P., Pank, K., et al. (2021). The medial offshore record of explosive volcanism along the central to eastern Aegean Volcanic Arc: 2. Tephra ages and volumes, eruption magnitudes and marine sedimentation rate variations. *Geochemistry, Geophysics, Geosystems*, *22*, e2021GC010011. https://doi.org/10.1029/2021GC010011

Received 1 JUL 2021
Accepted 14 OCT 2021

Author Contributions:

Data curation: K. Pank, J. C. Schindlbeck-Belo
Resources: T. H. Druitt, J. McPhie, P. Nomikou, S. R. Allen
Visualization: A. Freundt, K. Pank, J. C. Schindlbeck-Belo
Writing – review & editing: A. Freundt, T. H. Druitt, J. McPhie, P. Nomikou, K. Pank, J. C. Schindlbeck-Belo, T. H. Hansteen

The Medial Offshore Record of Explosive Volcanism Along the Central to Eastern Aegean Volcanic Arc: 2. Tephra Ages and Volumes, Eruption Magnitudes and Marine Sedimentation Rate Variations

S. Kutterolf[1], A. Freundt[1], T. H. Druitt[2], J. McPhie[3], P. Nomikou[4], K. Pank[1], J. C. Schindlbeck-Belo[1], T. H. Hansteen[1], and S. R. Allen[3]

[1]GEOMAR Helmholtz Centre for Ocean Research Kiel, Kiel, Germany, [2]CNRS, IRD, OPGC, Laboratoire Magmas et Volcans, Université Clermont Auvergne, Clermont-Ferrand, France, [3]School of Natural Sciences, University of Tasmania, Hobart, TAS, Australia, [4]Department of Geology and Geoenvironment, National Kapodistrian University of Athens, Athens, Greece

Abstract We use the tephrostratigraphic framework along the Aegean Volcanic Arc established in Part 1 of this contribution to determine hemipelagic sedimentation rates, calculate new tephra ages, and constrain the minimum magnitudes of (sub)plinian eruptions of the last 200 kyrs. Hemipelagic sedimentation rates range from ~0.5 cm/kyr up to ~40 cm/kyr and vary laterally as well as over time. Interpolation between dated tephras yields an eruption age of ~37 ka for the Firiplaka tephra, showing that explosive volcanism on Milos is ~24 kyrs younger than previously thought. The four marine Nisyros tephras (N1 to N4) identified in Part 1 (including the Upper (N1) and Lower (N4) Pumice) have ages of ~57 ka, ~63 ka, ~69 ka, and ~76 ka, respectively. Eruption ages for the Yali-1 and Yali-2 tephras are ~55 ka and ~34 ka, respectively. The Yali-2 tephra comprises two geochemically and laterally distinct marine facies. The southern facies is identical to the Yali-2 fall deposit on land but the western facies has slightly less evolved glass compositions. Overall, erupted plinian and co-ignimbrite fall tephra volumes range from <1 to 56 km^3 (excluding possible caldera fillings and ignimbrite volumes), and 80% of the eruptions had magnitude $5.5 < M \leq 7.2$ ($M = \log(m)-7$; m = erupted magma mass in kg). Twenty percent of the tephras represent $3.2 < M < 5.5$ eruptions. The long-term average tephra magma mass flux through highly explosive eruptions of Santorini is estimated at ~40 kg/s. The analogous data for the Kos-Yali-Nisyros volcanic complex is less-well constrained but similar to Santorini.

Plain Language Summary Sediment cores from the seafloor of the eastern Aegean Sea contain numerous ash layers from (sub)plinian eruptions from the Aegean Volcanic Arc that were correlated in Part 1. These correlations facilitate determination of sedimentation rates of ~0.5–~40 cm/kyr within the hemipelagic sediment bracketing the dated tephras. Sedimentation rates show temporal and lateral variations in the context of climate changes, and regional tectonics. Exceptionally high hemipelagic sedimentation rates within the last 4 kyrs, are linked to the 3.6 ka Minoan and the 1650 AD Kolumbo eruptions that emplaced abundant erodible tephra. Using the sedimentation rates we additionally determine the ages of hitherto undated tephras. We deduce an age of ~37 ka for a Milos eruption, as well as ~57 ka to ~76 ka for marine Nisyros and ~34 and ~55 ka for Yali tephras, for which previous dating attempts yielded controversial ages. The ash distribution in the marine realm of up to 10^5 km^2 represents a major fraction of the erupted tephra volumes that range from <1 to 56 km^3, placing 60% of the investigated eruptions into magnitude category M6, 20% into M7, and 20% into M3 to M5 classes. Over the past ~200,000 years, Santorini discharged magmas at an average rate of ~40 kg/s.

1. Introduction

Ash plumes of numerous plinian, phreatoplinian and ignimbrite-forming eruptions from calderas and stratocones of the central and eastern Aegean Volcanic Arc dispersed ash mostly eastward across the Aegean and Mediterranean seas (e.g., Keller et al., 1978). The resulting marine ash and lapilli layers represent the major fraction of the erupted tephra volumes because the relatively small volcanic islands in the Aegean Sea provide very limited onshore depositional areas (Figure 1). Such marine tephras have previously been sampled by sediment coring across the central and eastern Mediterranean at great distances from the source volcanoes. During RV Poseidon

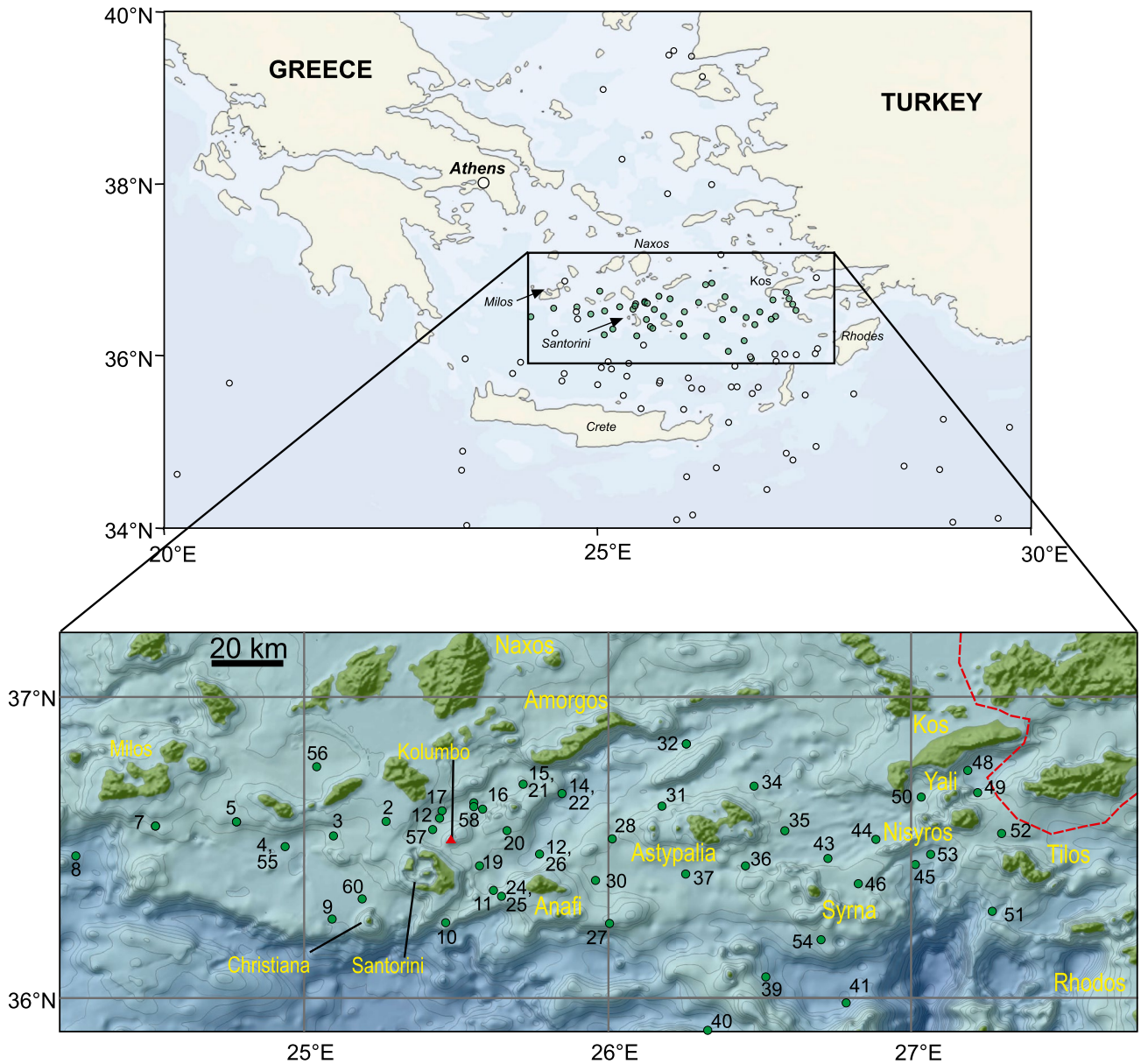

Figure 1. Topographic and bathymetric overview maps of the Aegean and northeastern Mediterranean region. Green dots on both maps mark the position of cores from RV Poseidon cruise POS 513. White dots of the overview map show previously investigated coring sites in the eastern Mediterranean region. On the close-up map of the eastern Aegean region, the red dashed line is the border between Greece and Turkey. Bathymetric contour interval is 1,000 m. Maps created using GeoMapApp (http://www.geomapapp.org; GMRT-Global Multi-Resolution Topography) (Ryan et al., 2009).

cruise POS 513 in 2017 (Freundt, 2017), we added to those distal data by collecting 47 sediment gravity cores along the volcanic arc at proximal to medial distances from their sources.

In Kutterolf, Freundt, Hansteen, et al. (2021), subsequently abbreviated as Part 1, we geochemically and stratigraphically correlated the marine ash layers between these cores and with tephras on land. We thereby identified 19 Pleistocene to Recent tephras from Milos, Santorini, Kolumbo, Kos, Yali and Nisyros volcanoes (Figure 1) that we could trace on the seafloor up to 300 km from their sources. In this second paper, we use the correlations to well-dated onshore tephras to determine regionally variable sedimentation rates of hemipelagic sediments intercalated with the marine ash layers. We then use these sedimentation rates to better establish the ages of tephras that have previously not, or only poorly, been constrained. Moreover, we combine published tephra isopach maps, based largely on outcrops on land, with the thickness data for marine tephra layers that can be traced across

several cores, to determine erupted tephra volumes and, hence, magnitudes of the large eruptions during the past 200 kyrs. Using the eruption ages and erupted tephra masses, we provide first estimates of long-term magma fluxes at the Aegean volcanic centers.

2. Geological Setting

2.1. The Aegean Volcanic Arc

The Aegean Sea conceals the subduction zone where the eastern Mediterranean lithosphere (front part of the African plate) subducts northeastward under the continental Aegean microplate with a velocity of ∼4 cm/yr. This setting makes the southern Aegean Sea one of the most tectonically active regions of western Eurasia (e.g., McKenzie, 1972; Papazachos et al., 2005; Shaw & Jackson, 2010). The Aegean microplate consists of thinned and strongly deformed continental crust, and is part of the Hellenic (Alpine) orogen that formed by a series of collisions with various lithospheric domains since the Jurassic (Zhu et al., 2006).

In the southern Aegean Sea (Cyclades), the upper crust is dominated by metamorphic units which formed during the Paleocene to Eocene by the obduction of the Apulian microplate (Bonneau & Kienast, 1982). Beginning at least in the Miocene, slab retreat and rapid southward migration of the Hellenic trench caused widespread extension in the southern and central Aegean region (Zhu et al., 2006). This extension resulted in significant crustal thinning, as manifested by the shallow Moho depth (∼25 km beneath Santorini; Makris et al., 2013), deep basins (e.g., the Cretan basin) and seismically active faults and grabens on the Aegean seafloor. Volcanic centers of the active Aegean Volcanic Arc are located in extensional neotectonic basins that cross-cut Plio-Quaternary sedimentary sequences (Pe-Piper & Piper, 2005). The Aegean Volcanic Arc stretches from the Gulf of Saronikos in the northwest to an area close to the Turkish coast in the east and includes the active volcanic centers at Methana, Milos, Santorini, and Nisyros (Figure 1). The distribution of volcanic centers and of eruptive vents follows strike-slip fault zones that are thought to facilitate the ascent of magmas (Nomikou, Papanikolaou, et al., 2013; Pe-Piper & Piper, 2005). The principal orientations are NE–SW at Santorini and Nisyros and NW–SE at Methana and Milos (Nomikou, Papanikolaou, et al., 2013). Large, composite volcanoes and volcano groups, including calderas (Milos, Christiana-Santorini-Kolumbo and Kos-Yali-Nisyros; Figure 1) characterize the central and eastern sectors of the arc (Francalanci et al., 2005) that we investigate here. These volcanoes produced large-magnitude eruptions of highly evolved, silicic magmas from the late Pleistocene through Holocene times (e.g., Allen & Cas, 1998; Cantner et al., 2014; Druitt et al., 1999; Fytikas et al., 1986; Hardiman, 1999; Stewart & McPhie, 2006; Wulf et al., 2020), depositing ash on the sea floor along the Aegean Volcanic Arc.

2.2. Onshore and Offshore Tephrostratigraphy of the Aegean Volcanic Islands

A number of publications have investigated the tephrostratigraphy of the Aegean volcanic islands (e.g., Allen & Cas, 1998, 2001; Allen & McPhie, 2000; Cantner et al., 2014; Druitt, 2014; Druitt et al., 1989, 1999; Druitt & Francaviglia, 1992; Fuller et al., 2018; Fytikas et al., 1986; Hardiman, 1999; Limburg & Varekamp, 1991; Stewart & McPhie, 2006; Wulf et al., 2020). The stratigraphy and ages of the Santorini tephra sequences are very well understood (e.g., Druitt et al., 1999; Wulf et al., 2020). In contrast, at the easternmost Kos-Yali-Nisyros (KYN) volcanic complex, the stratigraphy and ages of the two post-Kos-caldera volcanoes Yali and Nisyros are still the subject of discussion (Dietrich & Lagios, 2018; Tomlinson et al., 2012; Volentik et al., 2002). To date, Milos has not been known to have generated plinian eruptions but in Part 1 we demonstrated the existence of at least one widespread plinian tephra from Milos.

The Mediterranean seafloor sediments contain numerous tephra layers from Italian, Aegean and Anatolian volcanic sources which fortunately can be identified and distinguished by geochemical compositions. Numerous sediment drill cores (see Figure 1 in Part 1) have been used to establish the regional marine tephrostratigraphy of widespread tephra layers named according to the foraminifera zone in which they occur (e.g., Aksu et al., 2008; Albert et al., 2015; Bronk Ramsey, Albert, et al., 2015; Federman & Carey, 1980; Hardiman, 1999; Karkanas et al., 2015; Keller et al., 1978; Margari et al., 2007; Narcisi & Vezzoli, 1999; Paterne et al., 1990; Tomlinson et al., 2012, 2015; Vinci, 1985; Wulf et al., 2002, 2020). Well known examples from the Aegean region are tephra layer Z2 (Minoan Tephra), Y2 (Cape Riva Tephra), from Santorini and W3 (Kos Plateau Tuff) from Kos. Geochemical correlations between marine and onshore tephras have been greatly improved by the creation of compositional data bases (e.g., Bronk Ramsey, Albert, et al., 2015; Bronk Ramsey, Housley, et al., 2015; Satow

et al., 2015; Tomlinson et al., 2012, 2015; Wulf et al., 2004, 2008, 2012, 2020) to which we have added further major and trace element glass compositions of Aegean tephras from Part 1. The combination of our new data from the proximal and medial record with the distal marine tephrostratigraphy around the Aegean volcanic islands can be used to determine more accurate erupted volume estimates.

3. Methods

3.1. Marine Ash Layer Correlations

During RV Poseidon cruise POS 513 we collected 47 sediment gravity cores and 3 box cores in the Aegean Sea between Milos in the west and Nisyros in the east at water depths of ~100 to ~1,200 m (Figure 1). The cores contain 220 ash layers including primary ash layers and slightly reworked ash that retained its compositional integrity and stratigraphic position, identified by the criteria reviewed in Freundt et al. (2021). Glass geochemical compositions and relative stratigraphic positions were the major criteria by which we correlated these ash beds between cores and with tephras on land as discussed in Part 1.

3.2. Hemipelagic Sedimentation Rates and Tephra Ages

Ash layers correlated to dated onshore deposits provide time marks in the cores and the ages have the uncertainty of radiometric dating. We used these time marks, without including the one or two sigma errors from radiometric dating, to calculate average apparent sedimentation rates of the intercalated hemipelagic sediment (Figure 2). We subtracted the thickness of intercalated undated ash beds; these beds are typically thin (<10 cm) and cumulatively account for less than 5% of the core length. The thick tephra layers described in Part 1 all belong to dated tephras and have been excluded from the sedimentation rate calculations. We did not correct for the possible presence of dispersed ash in the hemipelagic sediment intervals because all sediment in the investigated region has a large terrigenous component including volcaniclastic material. By applying linear interpolation, we assumed that the hemipelagic sedimentation rates between two time marks remained constant over time. In many cases, the homogenous nature of the sediment justifies this assumption but there are also intervals which change from dark organic-rich to pale oxidized sediment, probably as a result of climatic changes that would have also modified hemipelagic sedimentation rates (e.g., Filippidi et al., 2016; Isler et al., 2016).

Errors in the sedimentation rates arise from the initial radiometric dating errors for the dated tephras (0.1–3 ka) as well as from uncertainty of defining the exact top of an ash layer that gradually changes from ash-rich to "normal" hemipelagic sediment. The largest radiometric dating errors translate into maximum errors of 0.5% to 5% for high and low sedimentation rates, respectively. The correlation of sapropels in our cores with well-dated sapropel horizons in the nearby ODP site 967 (Grant et al., 2017) provides independent age markers which support the sedimentation rates derived from tephra age anchor points. We preferred tephra time marks in our calculations because it is unclear if sapropels at the Aegean arc are perfectly synchronous with those at ODP site 967 (c.f. Rohling et al., 2015).

Using the calculated sedimentation rates, the ages of yet undated intercalated tephra layers can be estimated (Figure 2). These data lead to an age versus depth profile for each drilled core (Figure 3, Table 1; cf. Kutterolf, Freundt, Peréz, et al., 2008; Kutterolf, Freundt, Schacht, et al., 2008, 2016). An error in age up to 6% relative (Table S1 in Data Set S1) for the newly determined ages was estimated by performing this dating approach on tephras in several cores independently (cf., Kutterolf et al., 2013). This error includes uncertainties in the value and steadiness of sedimentation rates mentioned above. Errors arise from measurement uncertainties, non-steady sedimentation rates, and differential compaction in the uppermost part of the sediment. The new tephra ages provide additional support for stratigraphic correlations, particularly where geochemical correlations alone are uncertain.

3.3. Tephra Distribution, Volumes and Masses

In order to construct tephra isopach maps, we combined thickness data from our POS 513 cores with published thickness data from more distal Mediterranean cores and from studies of proximal tephra deposits on land. Since the offshore thickness data are sparse, the shape of the distal isopachs can only be roughly estimated, introducing some error into the volume calculations. The case study by Klawonn et al. (2014) showed that errors in volume calculations imparted by individuals' choices of contours applied to the same data set by 101 researchers with

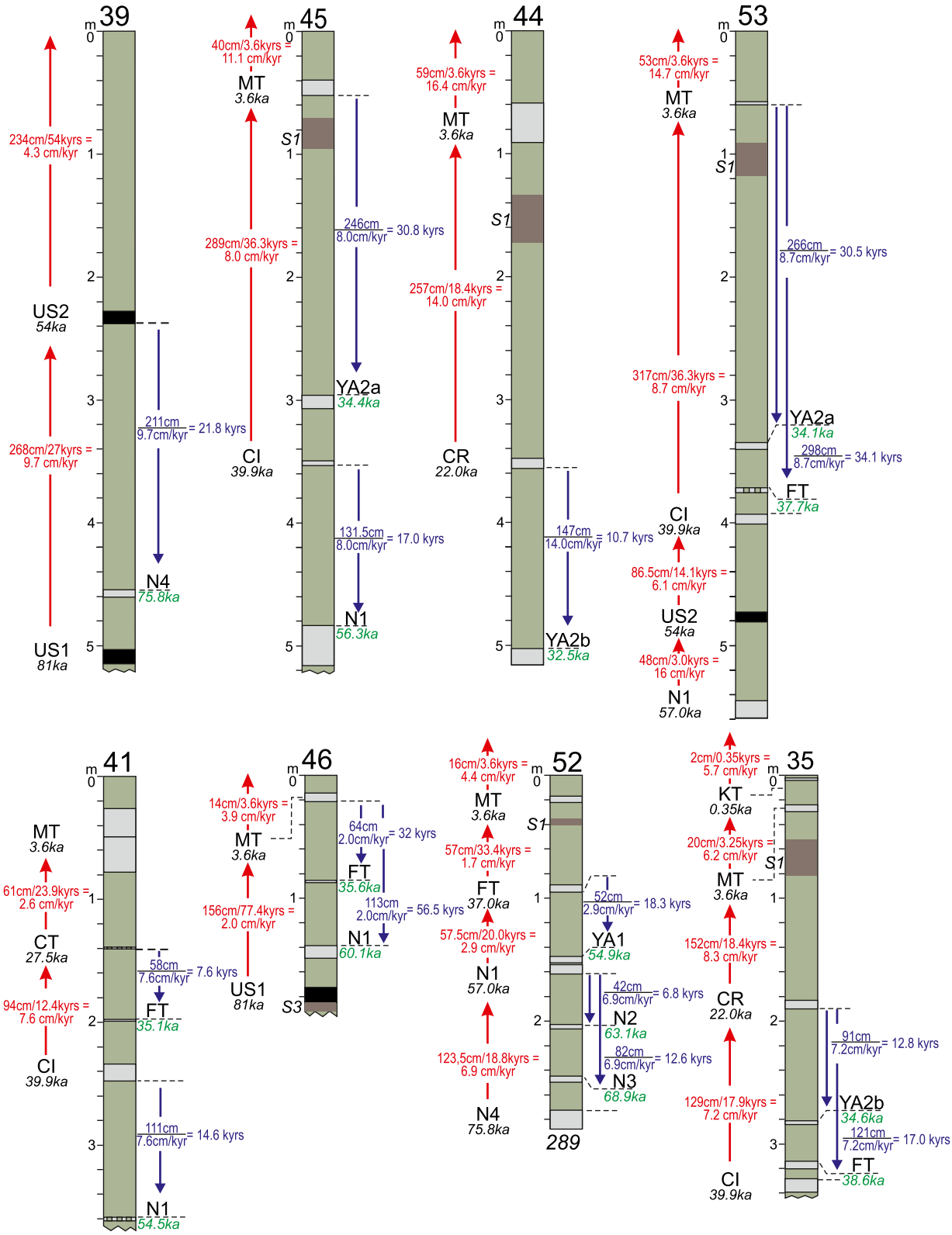
39
234cm/54kyrs = 4.3 cm/kyr
US2 54ka
268cm/27kyrs = 9.7 cm/kyr
US1 81ka
211cm 9.7cm/kyr = 21.8 kyrs
N4 75.8ka
45
40cm/3.6kyrs = 11.1 cm/kyr
MT 3.6ka
289cm/36.3kyrs = 8.0 cm/kyr
CI 39.9ka
S1
246cm 8.0cm/kyr = 30.8 kyrs
YA2a 34.4ka
131.5cm 8.0cm/kyr = 17.0 kyrs
N1 56.3ka
44
59cm/3.6kyrs = 16.4 cm/kyr
MT 3.6ka
257cm/18.4kyrs = 14.0 cm/kyr
CR 22.0ka
S1
147cm 14.0cm/kyr = 10.7 kyrs
YA2b 32.5ka
53
53cm/3.6kyrs = 14.7 cm/kyr
MT 3.6ka
317cm/36.3kyrs = 8.7 cm/kyr
CI 39.9ka
86.5cm/14.1kyrs = 6.1 cm/kyr
US2 54ka
48cm/3.0kyrs = 16 cm/kyr
N1 57.0ka
S1
266cm 8.7cm/kyr = 30.5 kyrs
YA2a 34.1ka
298cm 8.7cm/kyr = 34.1 kyrs
FT 37.7ka
41
MT 3.6ka
61cm/23.9kyrs = 2.6 cm/kyr
CT 27.5ka
94cm/12.4kyrs = 7.6 cm/kyr
CI 39.9ka
58cm 7.6cm/kyr = 7.6 kyrs
FT 35.1ka
111cm 7.6cm/kyr = 14.6 kyrs
N1 54.5ka
46
14cm/3.6kyrs = 3.9 cm/kyr
MT 3.6ka
156cm/77.4kyrs = 2.0 cm/kyr
US1 81ka
S3
64cm 2.0cm/kyr = 32 kyrs
FT 35.6ka
113cm 2.0cm/kyr = 56.5 kyrs
N1 60.1ka
52
16cm/3.6kyrs = 4.4 cm/kyr
MT 3.6ka
57cm/33.4kyrs = 1.7 cm/kyr
FT 37.0ka
57.5cm/20.0kyrs = 2.9 cm/kyr
N1 57.0ka
123,5cm/18.8kyrs = 6.9 cm/kyr
N4 75.8ka
S1
52cm 2.9cm/kyr = 18.3 kyrs
YA1 54.9ka
42cm 6.9cm/kyr = 6.8 kyrs
N2 63.1ka
82cm 6.9cm/kyr = 12.6 kyrs
N3 68.9ka
289
35
2cm/0.35kyrs = 5.7 cm/kyr
KT 0.35ka
20cm/3.25kyrs = 6.2 cm/kyr
MT 3.6ka
152cm/18.4kyrs = 8.3 cm/kyr
CR 22.0ka
129cm/17.9kyrs = 7.2 cm/kyr
CI 39.9ka
S1
91cm 7.2cm/kyr = 12.8 kyrs
YA2b 34.6ka
121cm 7.2cm/kyr = 17.0 kyrs
FT 38.6ka

Figure 2.

different education levels are around 8%, and thus relatively small, for well sampled intermediate-distance deposits, but increase with decreasing data density and with both distal and more proximal data sets. Thus, total tephra volumes have been obtained by different methods depending on available data quality and quantity.

Where sufficient data were available, we created ln (isopach thickness) versus square-root (isopach area) diagrams. We then applied the method of Pyle (1989) and Fierstein and Nathenson (1992) by fitting one or more straight lines to the data and subsequently integrating the functions to infinity. For some tephras, single straight lines provided a reasonably good fit to the data but other tephras required two or three separate straight-line segments to fit proximal through medial to distal data altogether. For comparison, we also applied the Weibull distribution function following Bonadonna and Costa (2012, 2013). This method commonly provides better fit to observed data and is particularly useful where the fitting of straight-line segments to the thickness versus area plots is ambiguous.

Methods for estimating volume have been developed for cases where tephra thickness data are too sparse to define a set of isopach lines. Green et al. (2016) applied a Bayesian statistical approach to sparse proximal and distal data, and Sulpizio (2005) tested three empirical methods to calculate distal tephra-fall volumes. Here we applied the method of Legros (2000) which yields a minimum tephra volume by assuming that the thickness at the farthest site lies on the dispersal axis and a tear-drop-shaped isopach with a pre-set aperture angle is fitted to it. We chose a 60° aperture angle for the eligible Aegean tephras because this aperture fits well-constrained isopachs of comparable deposits. Based on the assumption of an exponential thickness decrease, a minimum tephra volume can be determined by multiplying thickness by area.

We divided the total tephra volume into proximal and medial-distal partial volumes according to the patterns in ln (isopach thickness) versus square-root (isopach area) diagrams. We then accounted for the different interparticle pore spaces and lithic contents by reducing the proximal tephra volume by 50% ± 20% (onshore tephras) and the distal tephra volume by 30% ± 10% (marine tephras) (cf. Kutterolf, Freundt, & Peréz, 2008). The proximal reduction represents an average of crystal content (10–20 vol%) and lithic clast content (10–40 vol%), the variability of which between different phases of an eruption explains the error of ±20%. The juvenile particles building the remaining volumes have different densities proximally and distally. We measured the volumes of weighted pumice lapilli from proximal tephras by the sand-displacement method as described in Kutterolf et al. (2007), using four replicate measurements of batches of three lapilli for each tephra. Average onshore densities are 530 ± 100 kg/m^3, 680 ± 170 kg/m^3, and 1,030 ± 150 kg/m^3 for rhyolitic, dacitic and andesitic tephras, respectively. For the medial-distal volume, we determined the mean particle volumes of 31 weighted marine ash samples by dispersing the ash in water in a pycnometer. Uncertainty of ±10% in the volume determination reflects the averaged minor contribution of crystals and lithic clasts to the entire marine layer which is mostly <1 vol% in the bulk of the layers but can reach up to 20 vol% in a typically thin layer at the base. Subtracting visually estimated minor fractions of crystals and lithic fragments, we find the juvenile particle bulk densities to be 1,670 ± 250 kg/m^3 and 1,890 ± 210 kg/m^3 for felsic and mafic ash layers, respectively. Multiplying both, the proximal and distal volumes by the respective juvenile bulk densities yields the respective magma masses which add up to the total erupted magma mass for each eruption which, divided by the juvenile solid density, yields the dense rock equivalent (DRE) volume (Table S1 in Data Set S1).

We emphasize that we have determined only the volume of fall tephras, both plinian and co-ignimbrite, and therefore erupted tephra volumes are minima particularly for those eruptions that also produced significant pyroclastic density current deposits. We have not included volumes of pyroclastic density current deposits on land or on the sea floor unless they have been estimated independently (e.g., for the Kos Plateau Tuff), because their quantification would require additional work beyond the scope of our present study.

Figure 2. Schematic profiles of selected POS 513 cores indicating the positions of correlated tephra layers in each core (black = mafic ash, light gray = felsic ash, green = hemipelagic sediment, brown = sapropel). Uncorrelated and reworked tephra layers have been excluded for simplicity. Red arrows and associated numbers mark hemipelagic sediment intervals and their respective sedimentation rate calculated from the age difference between two dated ash layers and sediment interval thickness. Blue arrows and numbers indicate the time interval from a dated to an undated tephra layer, calculated as sediment thickness divided by sedimentation rate. Green italic numbers are the new tephra ages thus obtained. Previously dated tephras are marked by their age (italic numbers) and an acronym: KT = Kolumbo, KM = Kameni, MT = Minoan, CR = Cape Riva, CT = Cape Tripiti, US1 = Upper Scoriae 1, US2 = Upper Scoriae 2, CTh = Cape Thera, MP = Middle Pumice, LP1 = Lower Pumice 1, CT3 = Cape Therma 3, YA1 = Yali 1, YA2a,b = Yali 2, N1-N4 = Nisyros 1 to 4, KPT = Kos Plateau Tuff, FT = Firiplaka, CI = Campanian Ignimbrite.

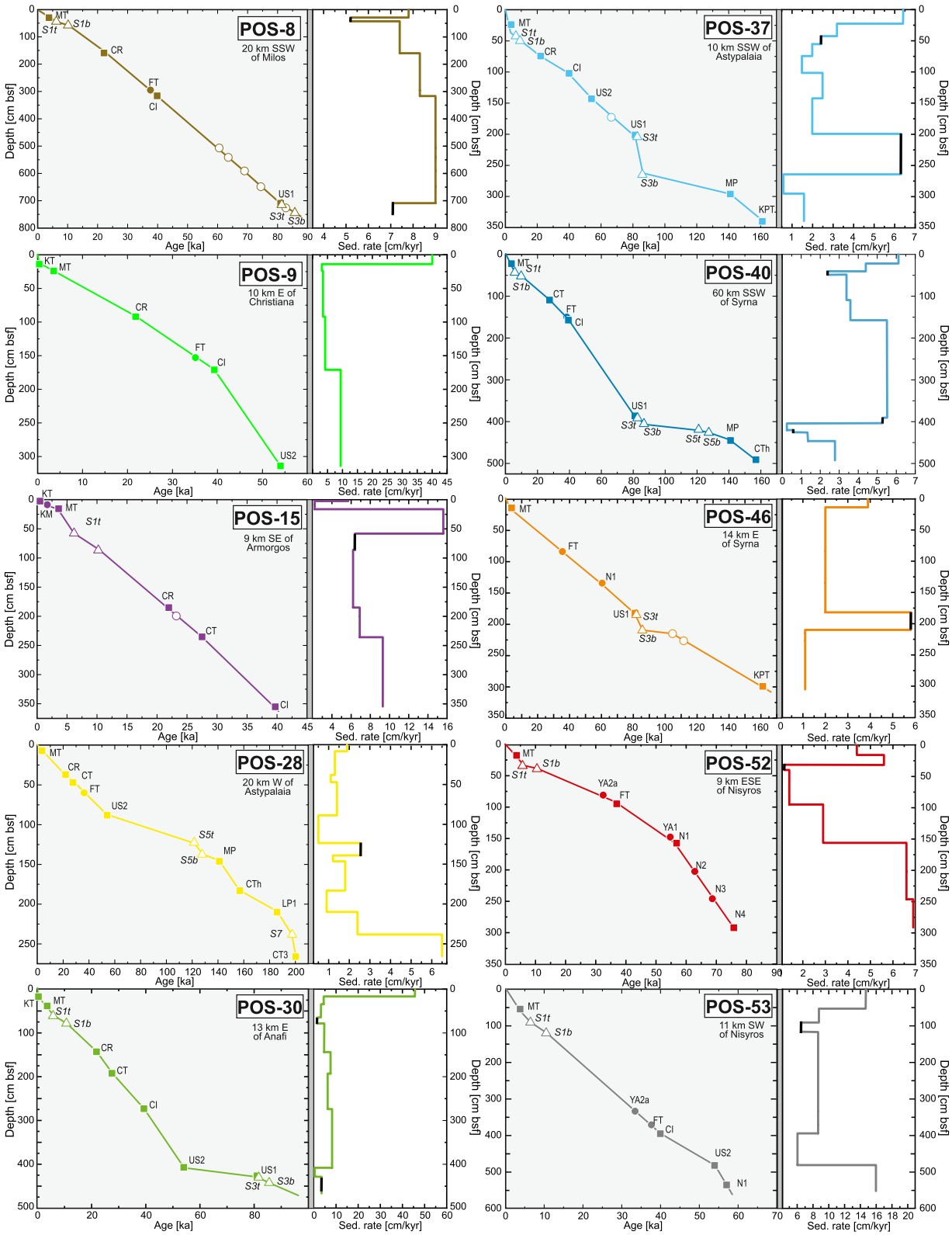
POS-8
20 km SSW of Milos
POS-37
10 km SSW of Astypalaia
POS-9
10 km E of Christiana
POS-40
60 km SSW of Syrna
POS-15
9 km SE of Armorgos
POS-46
14 km E of Syrna
POS-28
20 km W of Astypalaia
POS-52
9 km ESE of Nisyros
POS-30
13 km E of Anafi
POS-53
11 km SW of Nisyros
Depth [cm bsf]
Age [ka]
Sed. rate [cm/kyr]

Figure 3.

4. Sedimentation Rates

Figure 2 illustrates selected examples of hemipelagic sedimentation rates determined using the constraints from well-correlated and dated tephras bracketing hemipelagic sediment intervals. This approach yields variations in hemipelagic sedimentation rates with depth in cores that are long enough and contain sufficient suitable ash beds (Figure 3). Across all investigated cores, the observed range of sedimentation rates is 0.5–40 cm/kyr. However, rates >25 cm/kyr are exclusively found for the topmost sediment interval and are probably an artifact of a less compacted and soupy, water-rich material in the uppermost part of the core. Many cores contain dark sapropel layers (Figure 12, Part 1), which are commonly found across the Mediterranean and represent periods of deep-water anoxia (Rohling et al., 2015). The positions of sapropels are shown in Figure 3 (see also Table S2 in Data Set S1) using the sapropel ages S1 (6.1–10.5 ka), S3 (80.8–85.8 ka), S5 (121.5–128.5 ka), and S7 (197.53 ka) from Grant et al. (2017), where the age ranges give top and bottom ages, respectively. In most cases the sedimentation rate across a sapropel layer does not differ significantly from the hemipelagic sedimentation rate obtained from tephra ages around that interval; a notable exception is S3 in cores POS513-37 and -46 in which sedimentation rates are about three times those of surrounding hemipelagic sediment (Figure 3).

5. Ash-Layer Dating

The age range represented in our cores extends back to >200.2 ka, the time mark is set by the distal ash of the Cape Therma 3 eruption (Santorini; Wulf et al., 2020). Other time marks are given by the ash layers correlated with dated tephras on land. The age of yet undated ash layers can be estimated from their relative position between known time marks using linear interpolation as illustrated in Figures 2 and 3 (see also Table S1 in Data Set S1) and given with a 1-sigma uncertainty.

5.1. Milos

The ages of seven tephra layers, some of which can be correlated between cores over considerable distances (see Part 1), were previously not known or only very poorly constrained. One of these layers is the newly recognized Firiplaka Tephra (CA7) from Milos. The marine tephra has been correlated by chemical fingerprinting with three different onshore samples close to the Firiplaka volcano. In all cores, the marine tephra lies above ash layers from the 39.85 ka Campanian ignimbrite eruption (Giaccio et al., 2017), and below ash layers correlated with the 27.5 ka Cape Tripiti (Satow et al., 2015) or the 22 ka Cape Riva eruptions (Bronk Ramsey, Albert, et al., 2015). Recent Ar/Ar age dating of biotites from Milos suggested an age of 317 ± 4 ka for the Trachilas complex, an older pyroclastic sequence from Milos (Fytikas et al., 1986), and ages of 62 ± 3 ka, 70 ± 10 ka and 110 ± 20 ka for biotites from the upper and lower Firiplaka tephra sequence in the south of Milos (Zhou et al., 2021).

We dated ash layers of the Firiplaka Tephra (CA7) in 10 cores using sedimentation rates; the calculated ages range from 31.1 ka to 38.8 ka with an average age of 37.0 ± 1.3 ka (Figure 2, Table S1 in Data Set S1). This age is much younger than the Ar/Ar ages determined by Zhou et al. (2021), and is unambiguously constrained by the underlying 39.85 ka marine tephra of the Campanian Ignimbrite eruption. The discrepancy with the biotite-dating results may be related to excess argon problems in biotite but may also mean that the onshore tephra dated by Zhou et al. (2021) is from an older eruption of the Firiplaka volcano that did not, however, leave a trace in the investigated cores.

Figure 3. Sediment thickness versus age for selected POS 513 cores. Filled squares mark tephra layers of known age due to correlation with dated onshore tephras. Filled circles are tephra layers correlated with undated onshore tephras (cf. Figures 6 to 8 in Part 1). Open circles represent felsic and mafic ash beds the previously unknown age of which can here be constrained by their relative position between dated tephras. Sapropel (S) layers are marked by open triangles at the top (t) and base (b), using the respective age data from Grant et al. (2017). Right part of each age profile shows the variation of sedimentation rate with depth below sea floor, tephra thicknesses excluded. Black line segments represent sapropels. KT = Kolumbo, KM = Kameni, MT = Minoan, CR = Cape Riva, CT = Cape Tripiti, US1 = Upper Scoriae 1, US2 = Upper Scoriae 2, CTh = Cape Thera, MP = Middle Pumice, LP1 = Lower Pumice 1, CT3 = Cape Therma 3, YA1 = Yali 1, YA2a,b = Yali 2, N1-N4 = Nisyros 1 to 4, KPT = Kos Plateau Tuff, FT = Firiplaka, CI = Campanian Ignimbrite.

Table 1
Summary of Ages, Distribution, Eruption Volumes, and Eruption Masses for Agean Arc Eruptions Based on Marine Tephra Correlations

Eruption	Acronym	Volcanic complex	Age [ka]	Correlation #	Area [km^2] within (cm) isopach	1 segment volume* [km^3]	Multiple segments volume* [km^3]	Weibull volume# [km^3]	Magma mass [kg]	Magma volume (DRE) [km^3]	Eruption magnitude
Kolumbo	**KT**	Kolumbo volcano	***1650 AD*** [h]	**CA1**	**1.8 E^{+04}** (2)	**2.0**	**6.8**	**4.4**	**5.7 E^{+12}**	**2.5** [b]	**5.8**
Kameni	**KM**	Kameni island	***100 AD to 950 AD*** [K]	**CA2**	**1.1 E^{+03}** (2)	**0.2**	**0.06** [L]	**0.5**	**2.3 E^{+11}**	**0.4** [a]	**4.4**
Minoan	**MT**	Santorini	***3.6*** [h]	**CA3**	5.0 E^{+05} (2) [O]	44.8 [O]	46.7 [O]	53.1 [O]	7.8 E^{+13} [O]	32.4 [cO]	6.9 [O]
Cape Riva east	CR	Santorini	*22.0 ± 0.3* [x]	CA4	1.9 E^{+05} (2)	16.8	16.0	23.9	3.8 E^{+13}	16.0 [c]	6.6
Cape Riva north	CR	Santorini	*22.0 ± 0.3* [x]	CA4	1.8 E^{+05} (5)	34.4	n.a.	32.5	5.5 E^{+13}	22.8 [a]	6.7
Cape Riva total	**CR**	Santorini	***22.0 ± 0.3*** [x]	**CA4**	**n.a.**	**51.1**	**n.a.**	**56.4**	**9.3 E^{+13}**	**38.8** [b]	**7.0**
Cape Tripiti	**CT**	Santorini	***27.5 ± 0.7*** [s]	**CA5**	**1.4 E^{+04}** (1)	**1.2**	**1.6**	**3.1**	**5.3 E^{+12}**	**2.2** [b]	**5.7**
Yali 2a	Y2	Yali	*34.1 ± 0.4* [K]	CA6a	5.5 E^{+04} (2)	3.7	4.3	14.3	2.6 E^{+13}	11.0 [c]	6.4
Yali 2b	Y2	Yali	*34.6 ± 1.3* [K]	CA6b	8.0 E^{+02} (20)	0.6	n.a.	0.6	3.0 E^{+11}	0.1 [a]	4.5
Yali 2 total	**Y2**	Yali	***34.0 ± 0.9*** [K]	**CA6**	**n.a.**	**4.3**	**n.a.**	**14.7**	**2.7 E^{+13}**	**11.1** [b]	**6.4**
Firiplaka	**FT**	Milos	***37.0 ± 1.3*** [K]	**CA7**	**3.3 E^{+04}** (1.5)	**2.3**	**2.2**	**5.9**	**9.5 E^{+12}**	**4.1** [c]	**6.0**
Yali 1	**Y1**	Yali	***54.9 ± 2.2*** [K]	**CA9**	**6.6 E^{+02}** (3)	**3.4**	**n.a.**	**3.4**	**4.6 E^{+12}**	**2.0** [c]	**5.7**
Upper Scoria 2	**US2**	Santorini	***54 ± 3*** [f]	**CA10**	**1.1 E^{+04}** (3)	**1.2**	**1.4**	**5.8**	**9.3 E^{+12}**	**3.6** [b]	**6.0**
Nisyros 1 (Upper Pumice)	**N1**	Nisyros	***57.0 ± 2.9*** [K]	**CA11**	**4.8 E^{+04}** (3)	**5.6**	**6.9**	**16.6**	**2.9 E^{+13}**	**12.8** [c]	**6.5**
Nisyros 2	**N2**	Nisyros	***63.1 ± 2.5*** [K]	**CA12**	**1.7 E^{+02}** (4)	**0.007**	**n.a.**	**0.012** [L]	**1.7 E^{+10}**	**0.008** [a]	**3.2**
Nisyros 3	**N3**	Nisyros	***68.9 ± 2.7*** [K]	**CA13**	**1.6 E^{+02}** (5)	**0.008**	**n.a.**	**0.014** [L]	**2.0 E^{+10}**	**0.01** [a]	**3.3**
Nisyros 4 (Lower Pumice)	**N4**	Nisyros	***75.8 ± 3.0*** [K]	**CA14**	**2.9 E^{+03}** (4)	**0.7**	**0.8**	**2.3**	**3.3 E^{+12}**	**1.4** [c]	**5.5**
Upper Scoria 1	**US1**	Santorini	***80.8 ± 2.9*** [w]	**CA15**	**3.1 E^{+05}** (0.5)	**17.9**	**13.6**	**13.0**	**2.5 E^{+13}**	**9.8** [c]	**6.4**
Middle Pumice	**MP**	Santorini	***141.0 ± 2.6*** [w]	**CA16**	**3.4 E^{+04}** (3)	**4.3**	**4.0**	**9.2**	**1.4 E^{+13}**	**5.8** [c]	**6.1**
Cape Thera	**CTh**	Santorini	***156.9 ± 2.3*** [w]	**CA17**	**3.5 E^{+04}** (0.5)	**1.5**	**1.7**	**4.1**	**5.9 E^{+12}**	**2.2** [b]	**5.8**
Kos Plateau Tuff	**KPT**	Kos	***161.3 ± 2.2*** [t]	**CA18**	**5.3 E^{+05}** (1)	**24**	**16.9**	**33.1**	**4.6 E^{+13}**	**20.2** [b]	**6.6**
Kos Plateau Tuff total with IG	**KPT**	Kos	***161.3 ± 2.2*** [t]	**CA18**	**5.3 E^{+05}** (1)			**124.1**	**1.7 E^{+14}**	**71.1** [c]	**7.2**
Lower Pumice 2	**LP2**	Santorini	***176.7 ± 0.6*** [g]		**2.7 E^{+05}** (0.5)	**30.3**	**11.2**	**18.7**	**3.0 E^{+13}**	**11.6** [c]	**6.5**
Lower Pumice 1	**LP1**	Santorini	***185.7 ± 0.7*** [w]	**CA19**	**2.6 E^{+05}** (1)	**30.4**	**17.1**	**33.6**	**5.3 E^{+13}**	**20.4** [c]	**6.7**
Cape Therma 3	**CT3**	Santorini	***200.2 ± 0.9*** [w]	**CA20**	**2.9 E^{+04}** (2)	**4.8**	**4.5**	**5.5**	**7.9 E^{+12}**	**3.3** [b]	**5.9**

Note. volume determination after *Pyle (1989) and Fierstein and Nathenson (1992), #Bonadonna and Costa (2012) & (2013), [L]Legros (2000); [O]preliminary data from Karstens et al. in preparation; DRE volumes calculated with 2,300 kg/m^3 for rhyolitic magma, 2,400 kg/m^3 for dacitic magma, 2,600 kg/m^3 for andesitic magma. Radiometric and sedimentation rate ages from Friedrich et al. (2006) (h) Fabbro et al. (2013) (f), Bronk Ramsey, Albert, et al. (2015) (x), Gertisser et al. (2009) (g), Wulf et al. (2020) (w), Satow et al. (2015) (s), Smith et al. (1996) (t), h: historic ages. K: ages derived from sedimentation rates in this study. a: volumes based on distal ash only, b: volumes based on distal ash plus a minimum estimate of proximal volume, c: volumes based on distal ash and well-constrained proximal estimates. Non-bold values in the rows mark sub-phases of main eruptions, underlined values refer to ongoing work of the Minoan eruption, italic values represent ages and their errors for each eruption.

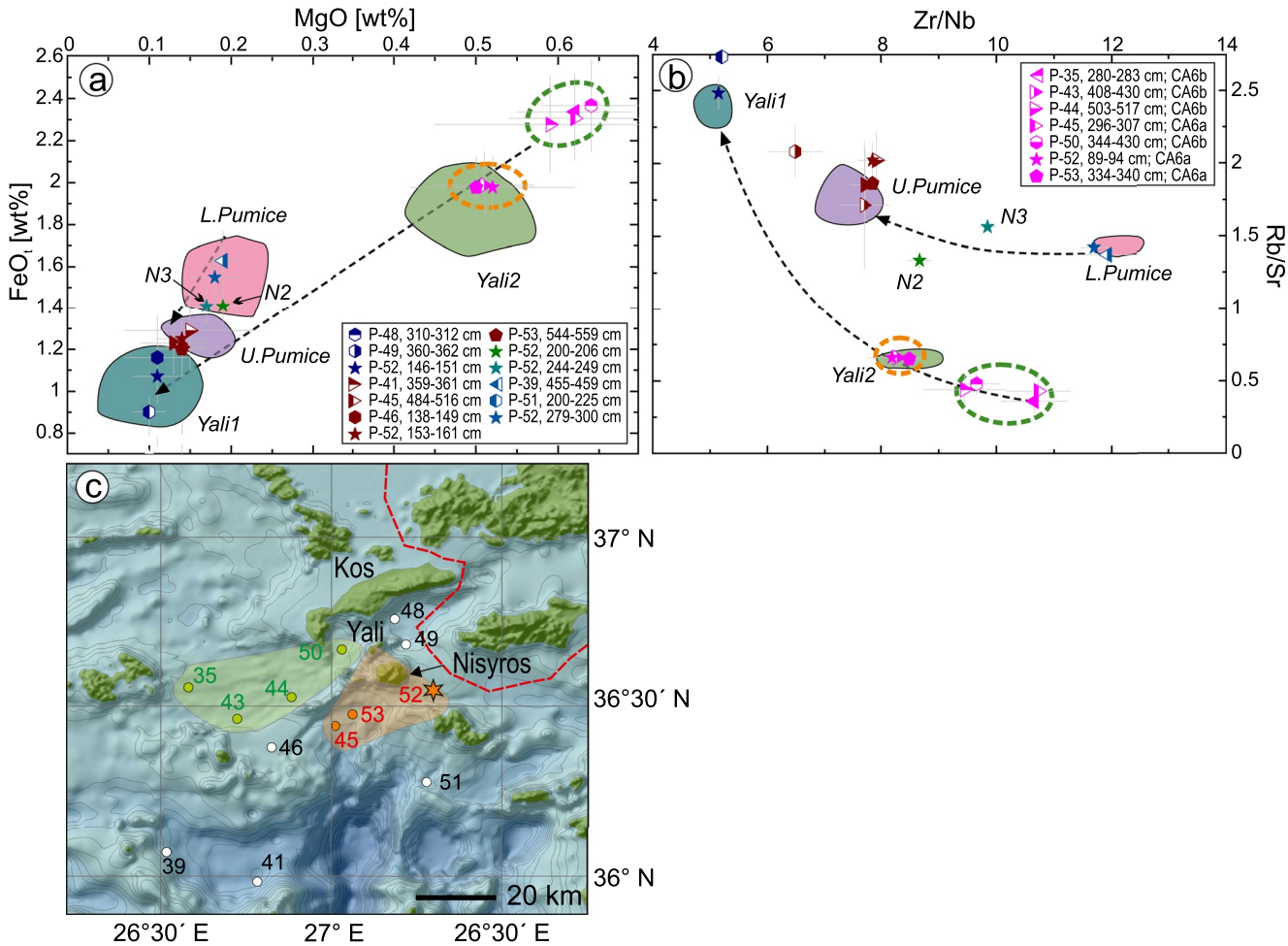

Figure 4. (a) Total FeO$_t$ versus MgO [wt%] (normalized to 100 wt% volatile-free composition) and (b) Zr/Nb versus Rb/Sr glass-compositional variations of onshore (colored fields) and marine (symbols) tephras from Nisyros and Yali. Onshore and marine geochemical data shown here are given in the supplement Tables S2a, S2b, S3a, and S3b of Part 1. Symbols are average values of all analyzed ash samples from a tephra, gray bars span the compositional range. Orange-dashed envelopes mark marine tephra facies Yali-2a which has the same glass composition as the Yali-2 fall tephra on land. Green-dashed envelopes include marine facies Yali-2b of less evolved glass composition. Dashed arrows emphasize different magmatic differentiation paths for Nisyros and Yali. However, in contrast to Nisyros, the most evolved Yali-1 composition had erupted long before the less-evolved Yali-2 magma. (c) Bathymetric map showing the positions of cores containing Nisyros and Yali tephras. Star symbol marks core POS 513-52 which contains all four Nisyros tephras N1 to N4. POS 513-52 and cores shown by orange dots contain Yali-2a facies which forms a southern fan (orange area). Green dots are cores containing Yali-2b facies which forms a western fan (green area). White dots are cores containing Nisyros tephras in addition to POS 513-52 and POS 513-53. Red dotted line shows the border with Turkey. Bathymetric contour interval is 600 m. Map created using GeoMapApp (http://www.geomapapp.org; GMRT-Global Multi-Resolution Topography) (Ryan et al., 2009).

5.2. Yali and Nisyros

The marine ash of the Yali-2 fall tephra (CA6a in Part 1) has been previously dated to 31 ka by oxygen-isotope stratigraphy (Federman & Carey, 1980). We found CA6a in three cores (POS 513-45, -52, -53) south of Yali (Figure 4c) from which we obtained an average age of 34.0 ± 0.5 ka by the interpolation method (Figure 2). The CA6a ash has the same glass composition as the Yali-2 tephra on land (Figures 4a and 4b; Figure 8 in Part 1).

In cores POS 513-35, -43, -44, and -50 west to southwest of Yali (Figure 4c), we found a tephra layer of slightly different glass composition (CA6b, Figures 4a and 4b) for which we obtained an average age of 34.0 ± 1.3 ka (Figure 2), which is identical to the CA6a age within error limits. The glass composition appears to represent a slightly less evolved version of the Yali-2/CA6a glass and is distinct in major and trace element composition from the Nisyros tephras (Figures 4a and 4b). We therefore interpret tephra layer CA6b as a compositionally distinct facies of the Yali-2 tephra that has not yet been recognized on land. Thus, we define a southern marine facies Yali-2a (Figure 4c) with glass composition the same as observed on land, and a western marine facies Yali-2b with

slightly less evolved glass composition. Combining the age determinations of both facies gives an average age for the Yali-2 eruption of 34.0 ± 0.9 ka (Figure 4, Table S1 in Data Set S1) which is close to the recent radiometric dating result (35 ± 2.8 ka) of Popa et al. (2020) that is based on U/Th disequilibrium ages of zircon.

Until recently the age of the Yali-1 pumice breccia (Allen & McPhie, 2000) could not be constrained because the base of the proximal deposit on land and underlying strata are not exposed, and so far radiometric ages had not been obtained. However, Popa et al. (2020) obtained zircon ages of 37.8 ± 9.5 to 41.3 ± 6.8 ka for Yali-1. The Yali-1 pyroclastic sequence comprises deposits from at least two major explosive and one minor explosive, as well as effusive events that are overlain by limestone which in turn is overlain by subaerial Yali-2 fall tephra and subaerial colluvial pumiceous sediments (Allen & McPhie, 2000). We found ash that can be correlated with the Yali-1 tephra using geochemical finger printing in three cores, one of which (POS 513-52) is constrained in age by sedimentation rate interpolation. This approach yields an Yali-1 eruption age of ∼54.9 ± 2.2 ka which is considerably older than the Popa et al. (2020) zircon eruption age. The reason for this discrepancy requires further investigation. We note that in core POS513-52 the compositionally correlated N1 tephra, which was dated on land by Popa et al. (2020) between ∼55 and ∼60 ka, is located only 5 cm below the Yali-1 tephra. If the ∼40 ka age from Popa et al. (2020) is correct, this sediment interval would have been emplaced at a very low sedimentation rate (0.25–0.33 cm/kyr) whereas our Yali-1 age would give a rate (0.9–10 cm/kyr), which is more compatible with the regional sedimentation-rate values (Figure 3).

Setting the Yali eruption ages in correct relation to the Nisyros eruption ages is important for understanding the magma evolution in the Kos-Yali-Nisyros magmatic system (Bachmann et al., 2010, 2012). Pyle and Margari (2009) argued that Yali-1 would be older than the caldera-forming eruption(s) of the Upper Pumice and Lower Pumice from Nisyros. However, the evolution of the Nisyros volcanic center is obscured by contradictions in published ages (Dietrich & Lagios, 2018; Tomlinson et al., 2012; Volentik et al., 2002). Specifically, published ages for the Lower Pumice from Nisyros (>70 ka to ∼29 ka) are incompatible with those for the Upper Pumice (>50 ka to 35 ka) (Karkanas et al., 2015; Limburg & Varekamp, 1991; Margari et al., 2007; Rehren, 1988; Tomlinson et al., 2012). Popa et al. (2020) recently published zircon crystallization ages of 54.9 ± 10.5 ka to 60.4 ± 3.9 ka for the Upper Pumice and 59.9 ± 17.1 ka to 74.3 ± 5.5 ka for the Lower Pumice; these ages overlap within the given error limits. As a result, the age of a major sector collapse event on Nisyros has not yet been well constrained (Anagnostopoulos & Anastasakis, 2021; Livanos et al., 2013; Tibaldi et al., 2008) and event frequencies used in volcanic hazard assessment remain uncertain (e.g., Kinvig et al., 2010; Nomikou et al., 2021; Seymour & Vlassopoulos, 1989).

The tephra correlations among the gravity cores (POS 513-39, 41, 45, 46, 48, 49, 51, 52 and 53; Figure 4c, Table S1 in Data Set S1) in the vicinity of Nisyros led to the definition of four tephra layers derived from Nisyros in Part 1 (Nisyros 1 to 4, top to bottom). Based on glass compositions, Nisyros 4 corresponds to the Lower Pumice (LPN) and Nisyros 1 corresponds to the Upper Pumice (UPN) whereas Nisyros 2 and 3 represent significant explosive eruptions in-between that have not yet been recognized on land. Application of the sedimentation-rate interpolation method to these cores yields an average age of 57.0 ± 2.9 ka for Nisyros 1 (Figure 2, Table S1 in Data Set S1), which lies within the zircon crystallization age range of the Upper Nisyros Pumice of Popa et al. (2020). Age determination for Nisyros 4 is only possible in one core (POS 513-39) where its calculated age of ∼75.8 ± 3 ka is well constrained by bracketing ash deposits of the 81 ka Upper Scoriae 1 and the 54 ka Upper Scoriae 2 tephras from Santorini (Figure 2, Table S1 in Data Set S1; ages from Fabbro et al., 2013; Wulf et al., 2020). Although less well constrained than the Nisyros 1 age, this Nisyros 4 age lies at the high end of the zircon crystallization age range determined by Popa et al. (2020). Applying our Nisyros 1 and 4 ages to core POS 513-52, the master core for the Nisyros (and Yali) marine succession because it contains all tephras in question (Figure 4c), we have determined ages of ∼63.1 ± 2 ka and ∼68.9 ± 3 ka for Nisyros 2 and 3, respectively.

5.3. Other Rhyolitic Tephras

Cores POS 513-7 and 8 south and southwest of Milos (Figure 1) contain up to four rhyolitic marine tephras of yet unknown origin because there are no onshore tephras with the same glass compositions in the reference database but chemical fingerprinting shows compositional affinity with Milos (see Part 1). Core POS 513-8 is much longer (744 cm) than core POS 513-7 (204 cm; Figure 12 in Part 1) and records a nearly constant hemipelagic sedimentation rate in the lower 4 m (Figure 3). It is thus well suited to estimate ages of the four tephra layers; their ages range from ∼61 ka to ∼82 ka. Major and trace element glass compositions suggest that the youngest of these

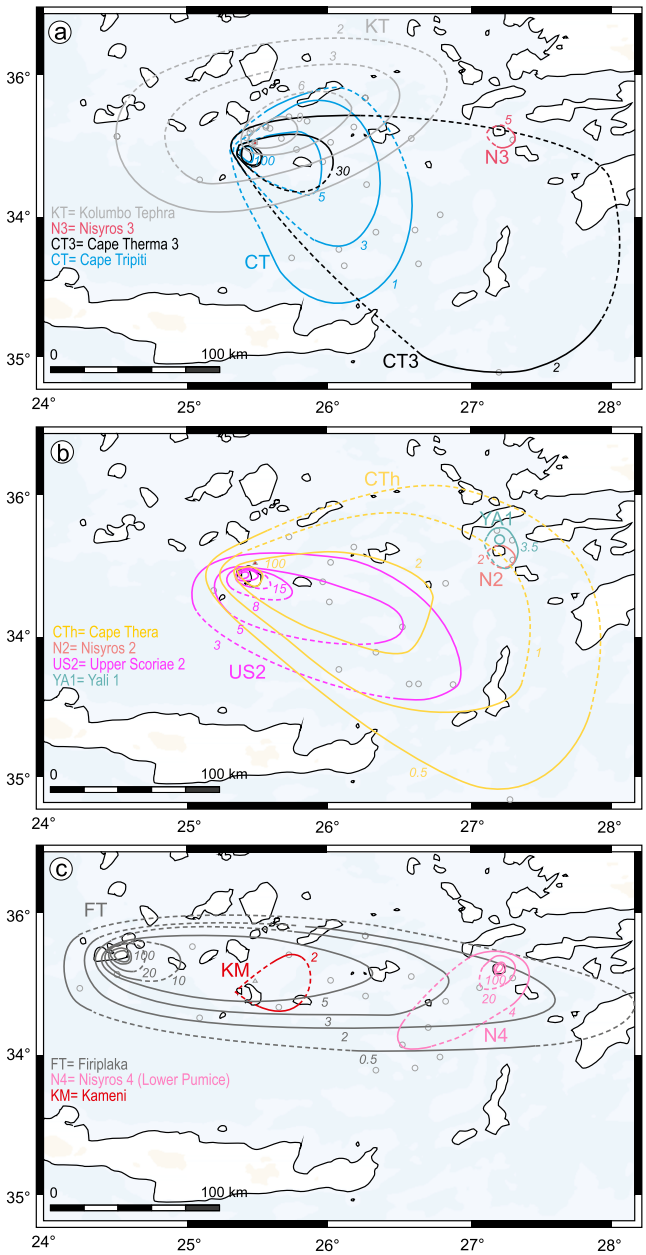

Figure 5. Isopach maps for the Aegean tephras. Italic numbers on isopachs indicate thickness in centimeters. (a) Kolumbo Tephra (KT), Cape Tripiti Tephra (CT), Cape Therma 3 Tephra (CT3), Nisyros 3 Tephra (N3). (b) Cape Thera Tephra (CTh), Upper Scoriae 2 Tephra (US2), Nisyros 2 Tephra (N2), Yali 1 Tephra (YA1). (c) Kameni Tephra (KM), Firiplaka Tephra (FT), Nisyros 4 Tephra (N4). Thickness values are given in Table S3 in Data Set S1, site coordinates are given in Part 1. We distinguish between well (solid lines) and poorly constrained (dashed lines) isopachs and note that the distal isopachs are constrained by variable numbers of available data (3–15 cores).

layers in core POS 513-8 (507–511 cm bsf, 60.5 ka) correlates with the oldest tephra at the base of core POS 513-7 (200–204 cm bsf, 50.5 ka), which thus gives an upper age limit for this core. The much shallower depth for this age in core POS 513-7, the observation that the tephra sequence from Kolumbo 1650 AD to Firiplaka 36 ka is concentrated in <40 cm core length, and the occurrence of unconformities in the upper part of the core indicate that the low apparent sedimentation rate at position POS 513-7 on the southern slope of Milos island (Figure 1) is probably due to mass wasting and removal of sediment.

6. Tephra Volumes and Magma Masses

Figures 5–7 show the isopach maps of tephras that are sufficiently widely correlated, based on the locations and thicknesses in respective cores (Table S2 in Data Set S1). The ln (thickness) versus square root (isopach area) data extracted from these maps and their functional fittings (Figure 8) give the tephra volumes summarized in Table 1. These estimates are probably still minima because very fine ash from large eruptions transported to distances far beyond the mapped area (e.g., Minoan and Cape Riva eruptions; Eastwood et al., 1999; Stanley & Sheng, 1986; Wulf et al., 2002) may have even shallower slopes on ln (thickness) versus square root (isopach area) diagrams, and hence the actual volumes are larger than those derived from extrapolation (e.g., Houghton et al., 2000).

In this section, we discuss every tephra according to the source volcanic centers in geographic order from west to east, using the correlations with marine ash layers CA1 to CA20 established in Part 1. We present here the most plausible tephra volumes resulting in most cases using the Weibull model (Bonadonna and Costa, 2012, 2013), or where data are sparse, the Legros model (Legros, 2000). We report the estimates generated by all applied methods in Table 1. Uncertainties in the fitting of straight lines to subsets of the tephra thickness versus area data mostly lead to underestimation of tephra volumes by 5%–50% compared to the Weibull method.

6.1. Milos

The marine tephra layer CA7, identified above as the 36 ka, rhyolitic Firiplaka Tephra, occurs as a 1- to 30-cm-thick ash layer in 15 of our POS 513 cores as well as in core TR172-26 of Hardiman (1999). However, the succession of compositionally similar tephras on land includes only small-volume local deposits of local extent and no proximal equivalent of a plinian tephra of that age has yet been identified on Milos. The deposits of the Firiplaka volcano have been divided into three stratigraphic units (Campos Venuti & Rossi, 1996; Fytikas et al., 1986; Stewart & McPhie, 2006) with ~0.2 km^3 total bulk volume. The lowermost unit includes pyroclastic fall deposits up to 2 m thick, but overall, the deposits are dominantly very lithic-rich pyroclastic density current deposits (Campos Venuti & Rossi, 1996). Based on the marine distribution of the Firiplaka Tephra, we estimate a minimum area (within the 1.5 cm isopach) of 3.3×10^4 km^2 and an erupted tephra volume of ~5.9 km^3, equivalent to ~4.1 km^3 DRE magma volume or $\sim 9.5 \times 10^{12}$ kg magma mass and a magnitude of M ~ 6.0 (Figures 5c, 8, Table 1 and Table S2 in Data Set S1).

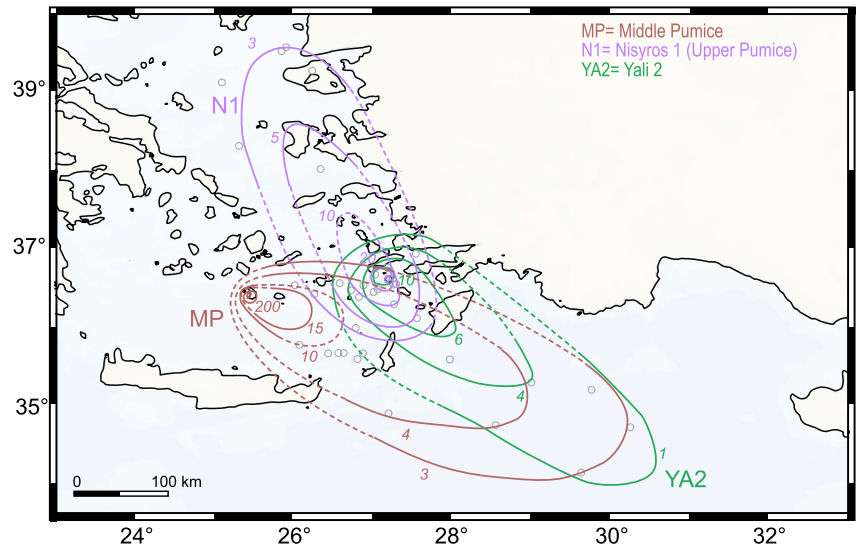

Figure 6. Isopach maps for the Aegean tephras (Santorini and Kos-Yali-Nisyros). Italic numbers on isopachs indicate thickness in centimeters. (a) Middle Pumice (MP), Nisyros 1 Tephra (N1), Yali 2 Tephra (YA2). Data source and other features as on Figure 5.

6.2. Santorini

Santorini caldera is the source of several widespread tephras (cf. Druitt et al., 1989, 1999, 2016; Gertisser et al., 2009; Keller et al., 2014, 1978; Simmons et al., 2017; Vinci, 1985; Wulf et al., 2020). Of these, we have correlated the Cape Therma 3, Lower Pumice 1 and 2, Cape Thera, Upper Scoriae 1 and 2, Cape Tripiti, Cape Riva, Minoan and Kameni tephras to marine tephras in the Eastern Aegean Sea in Part 1.

The Cape Therma 3 tephra layer, CA20, in marine core POS 513-28 (266–297 cm bsf) was also previously recognized in Meteor core KL51 (Wulf et al., 2020); distal data are scarce because most gravity cores did not reach sufficient depth. The 200.2 ± 0.9 ka old (Wulf et al., 2020) Cape Therma 3 tephra on the western coast of Thira is composed of 20-m-thick lag breccias (Druitt et al., 1999). By assuming the onshore thickness of 2 m of the Cape Therma 3 fall deposit reported in Druitt et al. (1999), including the two distal marine locations, and using the approach of Legros (2000), we estimate the minimum area within the 2 cm isopach to be 2.9×10^4 km^2, resulting in an erupted tephra volume of ~5.5 km^3, equivalent to 3.3 km^3 DRE magma volume or $\sim 7.9 \times 10^{12}$ kg magma mass and a magnitude of M ~ 5.9 (Figures 5a, 8, Table 1 and Table S3 in Data Set S1).

Ash layer CA19 (POS 513-28, 210–211 cm bsf) is correlated with the 185.7 ± 0.7 ka old (Wulf et al., 2020) onshore Lower Pumice 1, which is a thick composite fall (≤5 m) and flow (≤15 m) deposit on land, mainly exposed on southwestern Thira (Druitt et al., 1989, 1999; Simmons et al., 2016). This tephra also occurs in some other Mediterranean cores as ash layer V3 (e.g., Keller et al., 1978; Vinci, 1985; Wulf et al., 2020). Accordingly, this tephra covers an area of 2.6×10^5 km^2 (within the 1 cm isopach), corresponding to a tephra volume of 33.6 km^3, equivalent to 20.4 km^3 DRE magma volume or $\sim 5.3 \times 10^{13}$ kg magma mass and a magnitude of M ~ 6.7 (Figures 7a, 8, Table 1 and Table S3 in Data Set S1).

Although we did not find Lower Pumice 2 in our cores, it has been recognized in marine sediment cores to the south and southwest of Santorini (Keller et al., 1978). Facies and petrological characteristics of Lower Pumice 2 have been investigated in detail by Druitt et al. (1999), Gertisser et al. (2009), Keller et al. (2014), and Simmons et al. (2017). Lower Pumice 2 forms three distinguishable pumice fall units and a thin ash layer at the base (Gertisser et al., 2009; Keller et al., 2014) amounting to a ~20-m-thick, coarse grained, fall deposit in the western cliffs of Thira, overlain by several-meter-thick pyroclastic flow deposits (Druitt et al., 1999; Keller et al., 2014; Simmons et al., 2017). It has a thickness >1 m on Anafi, 30 km to the east of Thira (Keller et al., 2014). Using these data, we estimate a minimum area of 2.7×10^5 km^2 (within the 0.5 cm isopach), corresponding to a minimum tephra volume of 18.7 km^3, equivalent to ~11.6 km^3 DRE magma volume, or 3×10^{13} kg magma mass and a magnitude of M ~ 6.5 (Figures 7b, 8, Table 1 and Table S3 in Data Set S1).

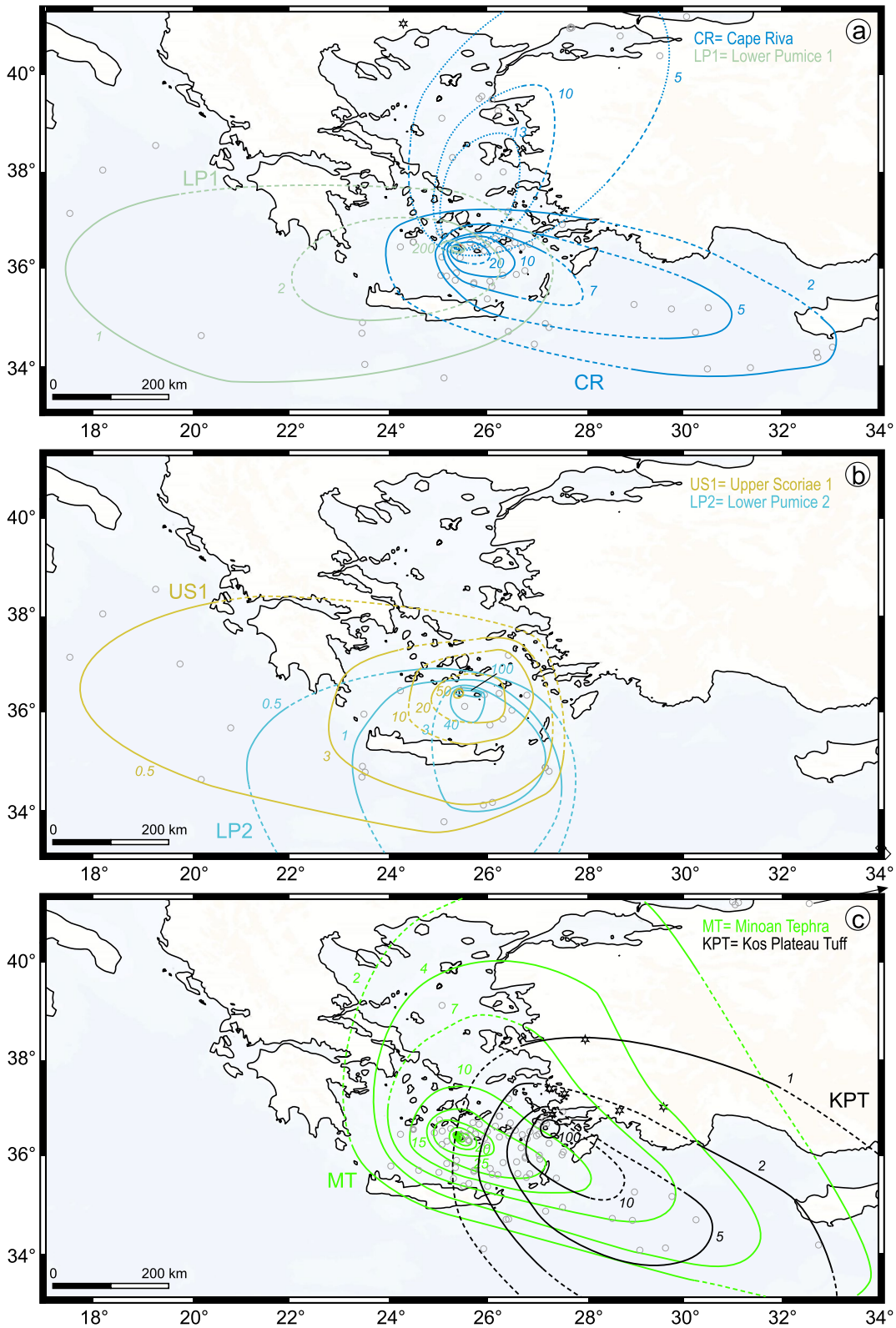

Figure 7. Isopach maps for four widespread Santorini tephras Italic numbers on isopachs indicate thickness in centimeters. (a) Cape Riva Tephra (CR) and Lower Pumice 1 (LP1). (b) Upper Scoriae 1 Tephra (US1) and Lower Pumice 2 (LP2). Data source and other features as on Figure 5. Several cm thick tephra from Cape Riva have also been found in Tenaghi Philippon (Seymour et al., 2004; Wulf et al., 2018), in the southwestern Black Sea (Kwiecien et al., 2008), and in western Turkey (Roeser et al., 2012). The data points have been considered for the isopachs and volume estimates but lie outside the map area.

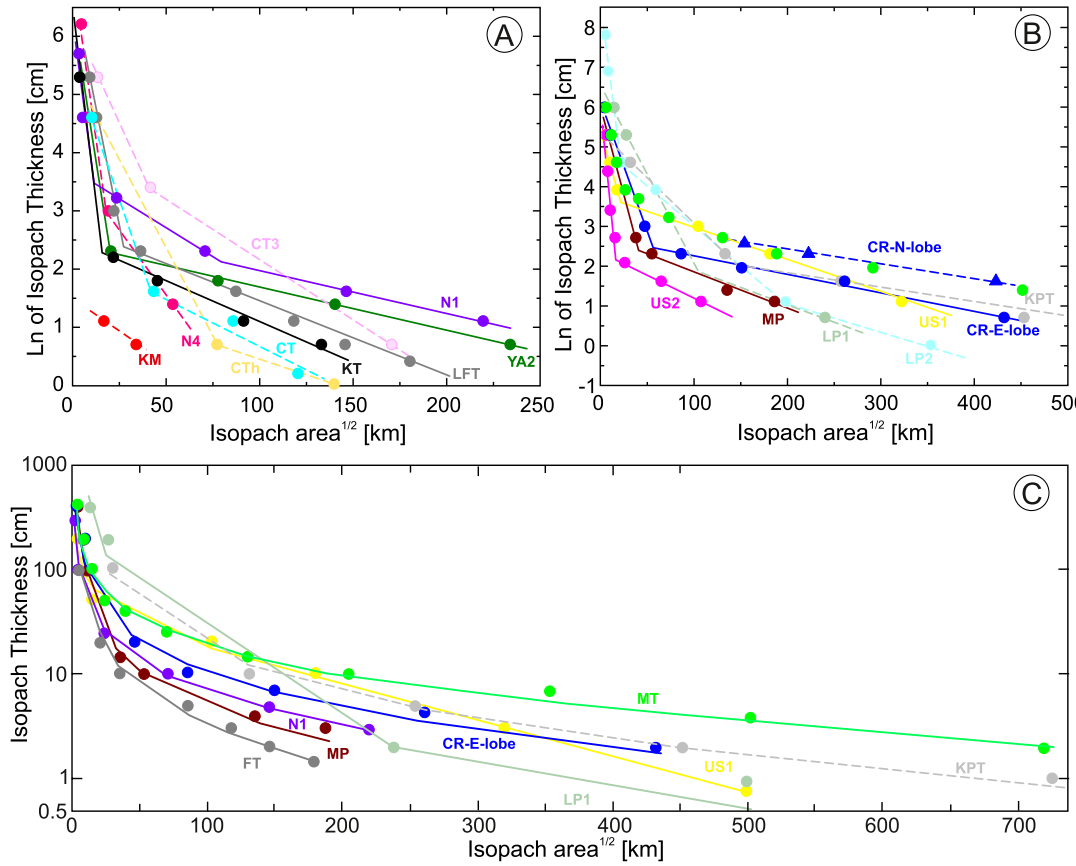

Figure 8. Natural logarithm of isopach thickness versus square-root of isopach area (Fierstein & Nathenson, 1992; Pyle, 1989) for all tephras mapped in Figures 5–7. (a) and (b) Fitting the data by two- or three-line segments works reasonably well for most tephras (solid lines); distribution into (a and b) due to the range of square-root isopach areas. However, data for KT, CR-north, KPT, CT, N4, CTh, LP1, LP2, CT3 (dashed lines) are only rough minimum estimates because the data are sparse and there are few well-constrained isopachs. (c) Fitting the data by the Weibull model of Bonadonna and Costa (2012, 2013), shown here exemplarily for the most widespread eruptions, generally yields a better fit and therefore more reliable volume estimate, particularly for tephras with more than three available isopachs. KT = Kolumbo, MT = Minoan, CR = Cape Riva with data for northern and eastern fans treated separately, CT = Cape Tripiti, US1 = Upper Scoriae 1, US2 = Upper Scoriae 2, CTh = Cape Thera, MP = Middle Pumice, LP2 = Lower pumice 2, LP1 = Lower Pumice 1, CT3 = Cape Therma 3, YA2 = Yali 2, N1, N4 = Nisyros 1, 4, KPT = Kos Plateau Tuff, FT = Firiplaka.

The Cape Thera eruption (156.9 ± 2.3 ka; Wulf et al., 2020) emplaced a basal pumice fall deposit (~85 cm thick) followed by a localized ignimbrite up to 60 m thick at the caldera walls (Druitt et al., 1999). We estimate a minimum of 1 m proximal fall tephra thickness. Together with the 2- to 4-cm-thick marine tephra layer, CA17, and marine thickness data from the southern Aegean and Mediterranean Sea (Hardiman, 1999; Wulf et al., 2020), we estimate the minimum area of the Cape Thera tephra to be 3.5×10^4 km^2 (within the 0.5 cm isopach). This area corresponds to ~4.1 km^3 tephra volume from fall deposit alone, equivalent to 2.2 km^3 DRE magma volume or ~5.9×10^{12} kg magma mass and a magnitude of M ~ 5.8 (Figures 5b, 8, Table 1 and Table S3 in Data Set S1).

The Middle Pumice (141.0 ± 2.6 ka; Wulf et al., 2020) is a complex succession of a compositionally zoned plinian fall deposit, densely welded at the caldera wall, and unwelded pyroclastic flow deposits including lag breccias (Druitt et al., 1999). The fall deposit is up to 10 m thick but is mostly 2–6 m thick along the caldera wall (Boyce & Gertisser, 2012; Sparks & Wright, 1979). The corresponding marine tephra layer, CA16, is 1–14 cm thick in POS 513 cores and has also been observed in other sediment cores by Federman and Carey (1980), Vinci (1985) and Wulf et al. (2020). Together, these data give a minimum area of 3.4×10^4 km^2 (within the 3 cm isopach; Figure 7) and a total fall tephra volume of 9.2 km^3, equivalent to 5.8 km^3 DRE magma volume or ~1.4×10^{13} kg magma mass and a magnitude of M ~ 6.1 (Figures 6a, 8, Table 1 and Table S3 in Data Set S1). This fall deposit volume is a minimum for the Middle Pumice eruption because the ignimbrite volume has not yet been determined.

The Upper Scoriae 1 tephra (80.8 ± 2.9 ka; Wulf et al., 2020) on land comprises fall and pyroclastic flow deposits extending across >60 km^2 on Thira (Druitt et al., 1989, 1999). The Upper Scoriae 1 eruption began with the emplacement of a widespread, 0.5- to 2-m-thick andesitic scoria fall deposit followed by breccias composed of spatter, bombs and lithic clasts up to 10 m thick; that layer is overlain by unwelded ignimbrite (Druitt et al., 1999; Mellors & Sparks, 1991). Marine tephra layer CA15 correlates with the Upper Scoriae 1 (Part 1) and occurs in six cores with thicknesses from 3 to 32 cm, typically within the sapropel S3 interval, as well as in other Mediterranean cores (Aksu et al., 2008; Hardiman, 1999; Keller et al., 1978; McCoy, 1981; Vinci, 1985; Wulf et al., 2020). Combining the onshore isopachs for Unit A fall deposit (Mellors & Sparks, 1991) with the marine data yields a minimum area (within the 0.5 cm isopach) of 3.1×10^5 km^2 (Figure 5) and a fall tephra volume (i.e., without the flow deposits) of ~13.0 km^3 equivalent to 9.8 km^3 DRE magma volume or $\sim 2.5 \times 10^{13}$ kg magma mass and a magnitude of M ~ 6.4 (Figures 7b, 8, Table 1 and Table S3 in Data Set S1).

Another prominent black marine ash layer, CA10, which is 7–12 cm thick in seven cores west and east of Santorini, is the marine equivalent of Upper Scoriae 2 on land. Using the data of Satow et al. (2015, 2020), we were able to identify US2 ash in their core LC21 southeast of Santorini. Wulf et al. (2020) observed US2 ash in core KL49 which lies closer to Santorini than LC21. The onshore Upper Scoria 2 deposits have a thin (<80 cm), widespread basal dacitic fall layer, overlain by andesitic pyroclastic surge deposits, lithic lag breccias, scoria flow deposits, and spatter agglomerates locally up to 50 m thick (Druitt et al., 1999; Mellors & Sparks, 1991). The Upper Scoriae 2 tephra covers a minimum area (within the 3 cm isopach) of 1.1×10^4 km^2, equivalent to ~5.8 km^3 erupted tephra volume, not including the proximal flow-deposit volume. This volume equates to ~3.6 km^3 DRE magma volume or $\sim 9.3 \times 10^{12}$ kg magma mass and a magnitude of M ~ 6.0 (Figures 5b, 8, Table 1 and Table S3 in Data Set S1).

The 27.5 ± 0.7 ka (Satow et al., 2015) dacitic Cape Tripiti eruption emplaced a 1-m-thick onshore pumice fall deposit mainly exposed on Therasia (Fabbro et al., 2013). This fall deposit continues as 1- to 7-cm-thick tephra layer CA5 on the sea floor and was sampled by seven POS 513 cores. It has also been identified in six other cores of the region (Y4 ash; Druitt et al., 1999; Hardiman, 1999; Keller et al., 1978; Satow et al., 2015; Vinci, 1985; Wulf et al., 2020). The marine and onshore thickness data constrain a minimum area of 1.4×10^4 km^2 (within the 1 cm isopach), giving an erupted tephra volume of ~3.1 km^3, equivalent to 2.2 km^3 DRE magma volume or $\sim 5.3 \times 10^{12}$ kg magma mass and a magnitude of M ~ 5.7 (Figures 5a, 8, Table 1 and Table S3 in Data Set S1).

The very widespread marine tephra layer, CA4, is the distal facies of the 22 ± 0.3 ka old Cape Riva tephra (Bronk Ramsey, Albert, et al., 2015), the rhyodacitic product of the third caldera-forming eruption of Santorini. On land, the Cape Riva tephra consists of a thick (~4 m), welded and unwelded pumice fall deposit (Cape Riva A) overlain by tens of meters of ignimbrite (Druitt, 1985; Druitt & Sparks, 1982). Marine tephra CA4 is found in 15 POS 513 cores. It is the Y2 layer of Keller et al. (1978) and has been identified in numerous other cores around the Aegean Sea (Aksu et al., 2008; Federman & Carey, 1980; Margari et al., 2007; Vinci, 1985; Wulf et al., 2002, 2020) but also in Tenaghi Philippon (Seymour et al., 2004; Wulf et al., 2018) and in the southwestern Black Sea (Kwiecien et al., 2008) and in western Turkey (Roeser et al., 2012). The thickness data suggests a bilobate fan (Figure 7); the grain size is overall finer at a given distance from the source in the northern compared to the eastern lobe. The eastern lobe has an orientation similar to most of the other Aegean Volcanic Arc fall tephras which were dispersed by high-level westerly winds. On the other hand, the occurrence of ~60-cm thick Cape Riva fall deposits on Eos (pers. com. Raphael Paris) and several cm-thick tephra in Tenaghi Philippon (Seymour et al., 2004; Wulf et al., 2018) as well as the absence of fall deposits under welded Cape Riva ignimbrite on eastern Thera suggest northward dispersal of the Cape Riva plinian fall deposit. However, further investigation is needed to clarify how the two dispersal lobes relate to changes in eruption mechanism and/or plume height. In the absence of reliable knowledge of their origin, we have estimated tephra volumes for the two lobes separately; the two lobes may be related to the two different eruption phases "CR-A/B" suggested by Wulf et al. (2002).

The onshore Cape Riva A fall data together with the marine data in the eastern lobe yields a minimum area of 1.9×10^5 km^2 (within the 2 cm isopach). The tephra volume of ~23.9 km^3 converts to 16.0 km^3 DRE magma volume or $\sim 3.8 \times 10^{13}$ kg magma mass (Figures 7a, 8, Table 1 and Table S3 in Data Set S1). The northern lobe is based mainly on the published distal data for the northern Aegean Sea and the Sea of Marmara (Aksu et al., 2008; Wulf et al., 2002). The ash covered a minimum area of 1.8×10^5 km^2 (within the 5 cm isopach), which amounts to ~32.5 km^3 tephra volume, 22.8 km^3 DRE magma volume or $\sim 5.5 \times 10^{13}$ kg magma mass (Figures 7a, 8, Table 1 and Table S3 in Data Set S1). Combining both eastern and northern ash volumes, the Cape Riva eruption released

a total of at least ~56.4 km^3 of fall tephra which does not include the unknown terrestrial proximal and distal marine ignimbrite volume. This fall deposit volume converts to ~38.8 km^3 DRE of magma volume or 9.3×10^{13} kg mass and a magnitude of M ~ 7.0 (Table 1).

The Minoan Tephra is up to 55 m thick on Santorini and comprises up to 5.5 m of a southeasterly dispersed fall deposit, divided into two subunits by grain-size characteristics, overain by a succession of syn-plinian pyroclastic surge deposits containing remnants of fall layers, and then by ignimbrite composed of several flow units (Druitt et al., 1999). The dominant white rhyodacitic pumice is accompanied by minor andesitic enclaves in the fall deposit. The marine tephra CA3, representing the 3.6 ka old Minoan tephra, is found in most POS 513 and in other Mediterranean sediment cores (Z tephra; Aksu et al., 2008; Federman & Carey, 1980; Hardiman, 1999; Keller et al., 1978; Margari et al., 2007; Satow et al., 2015, 2020; Vinci, 1985; Wulf et al., 2002, 2020) as well as in the southwestern and southeastern parts of the Black Sea (Kwiecien et al., 2008; Cullen et al., 2014). The fall tephra (which may include a co-ignimbrite component) covers 5×10^5 km^2 (within the 2 cm isopach) of the Aegean and eastern Mediterranean seas (Figure 6b) and yields a preliminary tephra volume of ~53.1 km^3 (Figures 7 and 8; Table 1). The preliminary erupted DRE magma volume is 32.4 km^3 and the corresponding magma mass is 7.8×10^{13} kg which yields a magnitude of 6.9 for the plinian phase of the eruption. Sigurdsson et al. (2006) interpreted a seismic facies observed around Santorini as the Minoan pyroclastic flow deposits and estimated their volume as 54.5 km^3 tephra or 41 km^3 DRE. These values need to be added to the fall values to characterize the total eruption volume. However, we refrain from doing that explicitly because ongoing work (e.g., Karstens et al., 2020) presently investigates new seismic data and investigate the dispersed ash part above marine tephra layers so that new ignimbrite volume estimates as well as more precise fall volumes will soon be published (Karstens, pers. com.).

Eruptions from Kameni Island between 100 and 950 AD generated marine tephra CA2, found up to 41 km from Santorini (Part 1). However, it is not possible to relate CA2 to a specific eruption and it is not clear whether all three separate ash layers were produced by the same or by different eruptions. Nevertheless, applying the Legros (2000) model to the sparse data provides a rough estimate of the magnitude of the Kameni eruptions. Tephra volumes in the range ~0.1–0.5 km^3 correspond to ~0.4 km^3 DRE magma volume or ~2.3×10^{11} kg erupted magma mass and a magnitude of M ~ 4.4 (Figures 5c, 8, Table 1 and Table S3 in Data Set S1).

6.3. Kolumbo

The youngest tephra layer identified in our cores (CA1) was produced by the 1650AD eruption of Kolumbo submarine volcano. We found this tephra in 16 POS 513 cores mostly to the east of the volcano where it is 6–73 cm thick and comprises proximal submarine pyroclastic density current and fall deposits and distal fall deposits from subaerial ash transport. We used data from Cantner et al. (2014) and Fuller et al. (2018) to estimate the proximal 20 m isopach at the crater wall and 2 m isopach at the foot of the edifice. Combined with our marine data, the minimum area for the Kolumbo Tephra (within the 2 cm isopach; Figure 5) is 1.8×10^4 km^2 and the total tephra volume is 4.4 km^3, corresponding to 2.5 km^3 DRE magma volume or 5.7×10^{12} kg magma mass and a magnitude of M ~ 5.8 (Figures 5a, 8, Table 1 and Table S3 in Data Set S1).

6.4. Kos

The phreatoplinian eruption of the Kos Plateau Tuff (KPT; 161.3 ± 2.2 ka, Smith et al., 1996) from a submarine vent was the largest eruption in the eastern part of the Aegean Volcanic Arc and formed a submarine caldera between Kos and Nisyros. An initial fall phase was followed by huge pyroclastic density currents which emplaced thick ignimbrite and surge deposits on Kos and other islands up to 160 km from the vent (Allen and Cas, 1998, 2001). The erupted magma volume responsible for caldera subsidence has been estimated as ~60 km^3 DRE (Allen et al., 1999; Nomikou, Croff Bell, et al., 2013). We correlated tephra layer CA18 in four POS 513 cores west of Kos with the KPT, and KPT ash has also been recognized in many other Aegean and Mediterranean cores by Federman and Carey (1980), Hardiman (1999), Margari et al. (2007), Satow et al. (2015, 2020), Vinci (1985), and Wulf et al. (2020) as well as in the southeastern Black Sea (Wegwerth et al., 2019). Using all these marine data, and the proximal thickness of fall unit A, the area (within the 1 cm isopach) is 5.3×10^5 km^2 (Figure 6b). The corresponding fall tephra volume is ~33.1 km^3. To this we add the ignimbrite volume of 91 km^3 for units B to F estimated by Allen et al. (1999) to derive a total erupted tephra volume of 124.1 km^3, corresponding

to 71.1 km^3 DRE magma volume or ~1.7×10^{14} kg magma mass and a magnitude of M ~ 7.2 (Figures 6b, 8, Table 1 and Table S3 in Data Set S1), which is within or slightly larger than previous estimates.

6.5. Yali

The exposed eruptive history of Yali volcano comprises submarine to emergent explosive and effusive activity represented by the >150-m-thick Yali-1 pumice breccia succession (~54.5 ka) which is separated by carbonate and clastic sediments from the ~34 ka Yali-2 subaerial pumice fall (Allen & McPhie, 2000). Yali-1 ash is present in three POS 513 cores east of Yali and Nisyros and is 2–5 cm thick. The area of within the 3 cm isopach is 660 km^2 (Figure 5b). Including a proximal area of ~9 km^2 and minimum thickness of 75 m evident from profiles shown in Allen and McPhie (2000) across southern Yali island, we estimate the erupted tephra volume to be ~3.4 km^3, the erupted magma volume to 2.0 km^3 DRE and the erupted magma mass to be 4.6×10^{12} kg corresponding to a magnitude of M ~ 5.7 (Figures 5b, 8, Table 1 and Table S3 in Data Set S1). The rather limited lateral dispersal of Yali-1 ash seems to contrast with the impressive thickness of the proximal deposits. Where it is thickest (POS 513-52), the Yali-1 ash consists of four normally graded medium to fine ash layers with boundaries at low angles to each other, suggesting deposition from submarine density currents.

As discussed above, the marine ash related to the Yali 2 eruption comprises two contemporaneous facies distinguished by glass composition and western and southern dispersal (Figure 4c). The 3- to 11-cm-thick southern facies (Yali-2a) is massive, rather well-sorted, normally graded fine lapilli to coarse ash. The western facies (Yali-2b) is massive, 3–22 cm thick fine ash in three cores but in core POS513-50 closest to Yali island, it is an 86-cm-thick bed of multiply graded medium to fine lapilli overlain by stratified ash (Figure 4c). Using a minimum thickness of 2 m on Yali and Nisyros (Allen & McPhie, 2000), 3–11 cm thicknesses in POS 513 cores and 1-to 9-cm-thick Yali 2 ash layers observed in other, more distal cores (Aksu et al., 2008; Hardiman, 1999; Satow et al., 2015; Vinci, 1985), we estimate the minimum area to be 5.5×10^4 km^2 (within the 2 cm isopach; Figure 6a). The tephra volume for the fall facies (Yali-2a) is 14.3 km^3, corresponding to 11.0 km^3 DRE magma volume or 2.6×10^{13} kg magma mass and a magnitude of M ~ 6.4 (Figures 6a, 8, Table 1 and Table S3 in Data Set S1). For Yali-2b facies, we obtain significantly lower values of 0.6 km^3 tephra volume and 0.1 km^3 DRE magma volume or 3×10^{11} kg magma mass. In total this sums up to a tephra volume of 14.7 km^3, corresponding to 11.1 km^3 DRE magma volume.

6.6. Nisyros

For the Upper and Lower Pumice from Nisyros, dated herein at ~57 ka and 75.8 ka, respectively, we use onshore thickness data from Hardiman (1999). Distal marine thickness data from the literature are available only for the Upper Pumice tephra (Aksu et al., 2008; Karkanas et al., 2015; Margari et al., 2007; Tomlinson et al., 2012; Vinci, 1985). Nisyros 1, the marine tephra of the Upper Pumice from Nisyros, is 2–53 cm thick and present in 13 marine gravity cores from near Nisyros Island to 300 km downwind in the northern Aegean Sea, resulting in a minimum area of 4.8×10^4 km^2 within the 2 cm isopach. The erupted tephra volume estimate of 16.6 km^3 corresponds to 11.8 km^3 DRE magma volume or 2.9×10^{13} kg of magma mass and a magnitude of M ~ 6.5 (Figures 6a, 8, Table 1 and Table S3 in Data Set S1).

We found Nisyros 4 marine tephra, equivalent to the Lower Pumice from Nisyros, in one core close to the south of the island (thickness >20 cm) and another distal core to the southwest (4 cm thickness). The minimum area within the 4 cm isopach is 2,860 km^2 (Figure 5c). The tephra volume of ~2.3 km^3 corresponds to 1.4 km^3 DRE magma volume or 3.3×10^{12} kg magma mass and a magnitude of M ~ 5.5 (Figures 5c, 8, Table 1 and Table S3 in Data Set S1).

The newly identified marine tephras, Nisyros 3 and Nisyros 2, intercalated between Nisyros 4 and Nisyros 1, occur in one core only (POS 513-52) southeast of Nisyros (Figure 1) and no equivalent deposit has yet been found on land. We thus used the minimal data approach of Legros (2000), assuming the core site 15 km from the island lies on the axis of a dispersal fan with 45° aperture. This approach gives a rough estimate of minimum tephra volume of ~11×10^6 m^3 (2.01×10^{10} kg magma) for the 4-cm-thick ash layer Nisyros 3 (CA13) and ~9×10^6 m^3 (1.72×10^{10} kg magma) for the 3-cm-thick ash layer Nisyros 2 (CA12) corresponding to magnitudes of M ~ 3.2 and 3.3 (Figures 5a, 5b, 8, Table 1 and Table S3 in Data Set S1).

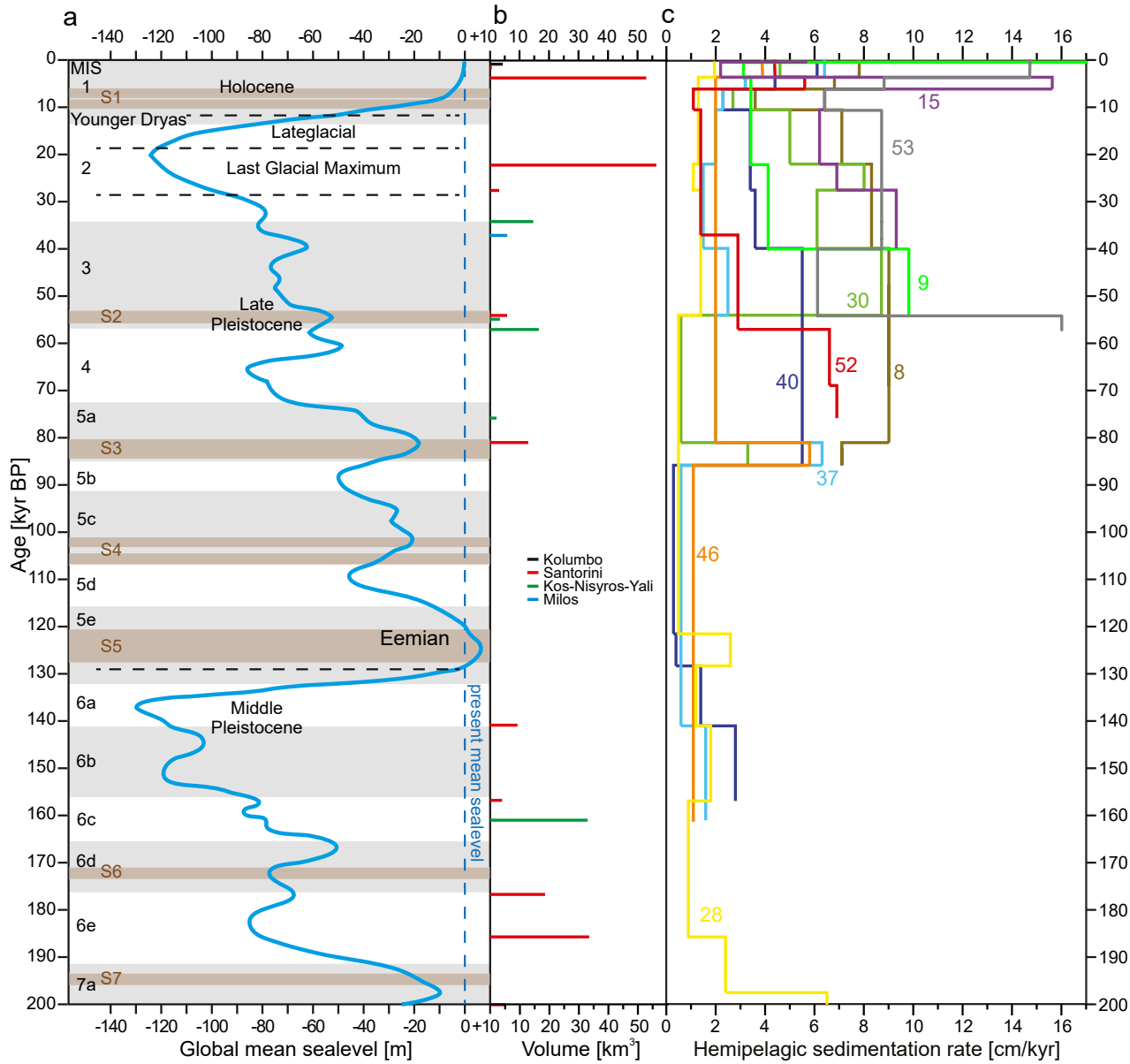

Figure 9. (a) Temporal variation of global mean sea level (blue curve) after Benjamin et al. (2017) and Waelbroeck et al. (2002). Brown bars indicate sapropels S1 to S7 after Grant et al. (2017), Kroon et al. (1998) and Rohling et al. (2015). Gray - white alternations mark marine isotope stages MIS 1–7 after Railsback et al. (2015). (b) Minimum emitted tephra volumes of the major Aegean eruptions. Note that particularly the large-volume fall deposits were associated with additional large-volume ignimbrites not considered here. (c) Variation of hemipelagic sedimentation rates analogous to Figure 3 but varying with age rather than depth in core. Age anchor points and sedimentation rates are summarized in Table S2 in Data Set S1.

7. Discussion

7.1. Significance of Sedimentation-Rate Variations

The correlated tephras provide excellent time marks that facilitate to determine the average sedimentation of hemipelagic sediment between them, and hence lateral and temporal variability in these rates in the relatively shallow waters along the Aegean arc. We have not investigated the sediments in any detail, apart from the obvious division into light hemipelagic and dark sapropel intervals, but we think that our data provide a first insight into how sedimentation rates were possibly affected by climate changes, eruptive events and tectonic activities. Variations of hemipelagic sedimentation rates in selected cores (Figure 3) are compared with environmental parameters such as sea level changes and sapropel intervals in Figure 9. It should be noted that the temporal

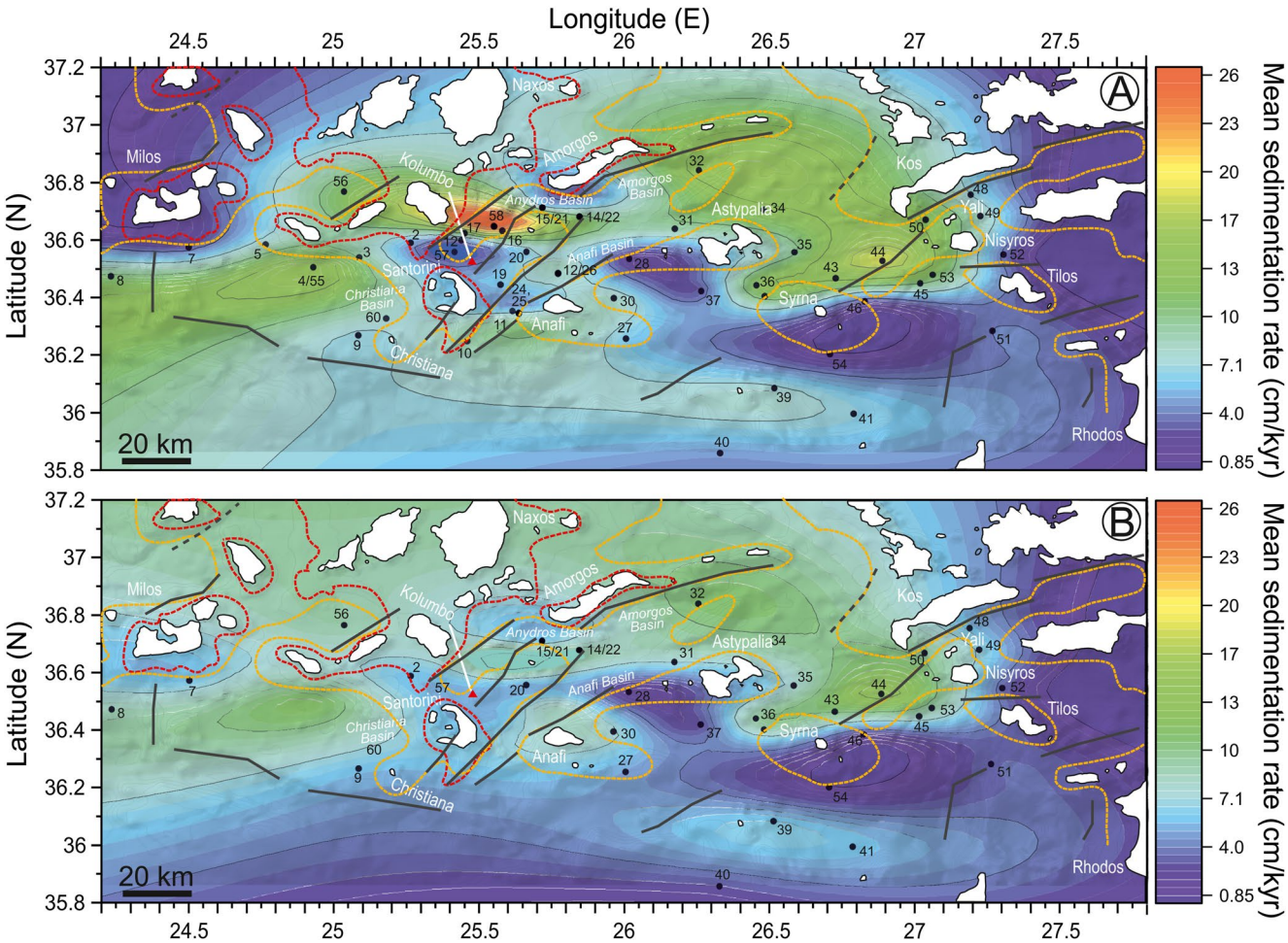

Figure 10. Lateral distribution of average hemipelagic sedimentation rates across the eastern Aegean region for the time periods (a) 0–60 ka and (b) 4–60 ka. Core positions are indicated by black dots with black core numbers. Present day islands are shown as white fields. Red dashed line is the coast line during the Last Glacial Maximum (~20–30 ka; Figure 9a), yellow dashed line is the estimated coast line during the Middle/Late Pleistocene glacial maximum (~140 ka; Figure 9a), and gray lines are major faults, all from Sakellariou and Galanidou (2016). At least near the positions of cores POS513-28 and -46 Middle Pleistocene regression is overestimated because these cores contain marine sediments of that age. Sedimentation rate contours (color shaded areas) were generated with the contouring app of Origin 2021 and superimposed on the bathymetric map of Figure 1. Note that contours outside a tight envelope around the core positions are calculation artifacts.

resolution of the sedimentation rates profiles is much less than that of sea level variations, and that comparisons must be made with some caution.

Very low sealevel during the last two Pleistocene glacial maxima created much larger erodible land surface and longer coastlines around the Aegean arc (Figure 10; Sakellariou & Galanidou, 2016, 2017; Simaiakis et al., 2017). None of our cores, however, shows significantly increased sedimentation rates during these periods (Figure 9), possibly because drier climate reduced erosion rates on land. On the other hand, high sealevel conditions of the Eemian interglacial lasting from ~120 ka until about 80 ka, also did not produce elevated sedimentation rates in the four cores that crossed this interval even though stronger erosion would be expected during warmer and wetter climate (Cane et al., 2002; Rohling et al., 2015). One possible exception may be the slightly elevated rate across sapropel S5 in core POS513-28 near Astypalia. For the warm, relatively wet high-sealevel Holocene period all cores show elevated sedimentation rates between 6.5 and 3.6 ka, that is, from the top of sapropel S1 up to the Minoan tephra, similar to the rates below sapropel 1. Sedimentation rates within sapropel S1 (Figure 9, Table S2 in Data Set S1) are generally lower. Sapropel S3 is present in five cores but only two of these (cores POS513-37, -46) yield elevated sedimentation rates for the S3 interval. Although the sedimentation rates of the Aegean sapropel intervals roughly agree with those found at ODP967 south of Cyprus (S1 6.6 cm/kyr, S3 5.2 cm/kyr; Grant

et al., 2017), they vary widely between cores (S1 1.1–13.6 cm/kyr, 16 cores; S3 3.3–7.1 cm/kyr, 5 cores) probably in response to the varied paleomorphology along the Aegean arc.

Subaerial and submarine erosion rates can also be greatly enhanced when explosive volcanic eruptions emplace large volumes of easily erodible tephra. For example, Zhao et al. (2019) documented very high erosion rates immediately after emplacement of the Capelinhos cone (Faial, Azores) that declined in inverse power-law fashion through later times. However, none of the cores in the central Aegean region shows a significant increase in sedimentation rate after the largest eruptions on Santorini, nor is such feature observed in the eastern cores after the Kos, Nisyros and Yali eruptions (Figure 9). In many cores there is an apparent increase in sedimentation rate between the Minoan ash and the seafloor that may be partly due to uncompacted nature of near-seafloor sediment; some cores even show a reverse trend of lower rates immediately below the sea floor. For the older eruptions, the absence of post-eruptive sedimentation-rate peaks may be a problem of temporal resolution. For example, the hemipelagic sedimentation rate after the Cape Riva eruption is determined as the average rate of the time interval 22-3.6 ka. Such averaging would obscure an initial, relatively short-lived peak in sedimentation rate that is followed by a relatively long period of low and declining sedimentation rates. Dedicated petrographic analysis of the sediments may eventually resolve such features.

Tectonic uplift increases erosion rates and may be visible as enhanced sedimentation rates in surrounding seafloor profiles. The fast uplift of Yali (discussed in Section 7.2) did not, however, produce obviously elevated sedimentation rates in sediment cores around the Yali-Nisyros complex. Since the Yali-1 eruption, sedimentation rates in core POS513-53 remained approximately constant whereas those in core POS513-52 actually declined (Figure 9).

Figure 10 shows the lateral distribution of the average hemipelagic sedimentation rate for the past 60 kyrs, ignoring the local temporal variations during that period which are, in most cores, limited in magnitude except for the topmost zone (Figure 3). This regional comparison shows that the average rate is relatively high in the basin west of Yali. Future studies investigating the proportion of Yali-derived volcaniclastic material in the sediments may reveal whether these high values can at least partly be attributed to tectonic uplift of Yali.

The distribution map shows an even more prominent maximum in hemipelagic sedimentation rate north of Kolumbo volcano. This area overlaps with the Anydros tectonic basin which forms a sediment sink that subsided in a stepwise fashion (Fuller et al., 2018; Hübscher et al., 2015; Nomikou et al., 2016). The sedimentation rate maximum in Figure 10a is strongly reduced when the last 4 kyrs are excluded from the averaging (Figure 10b). This reduction is presumably mainly due to deposition of Kolumbo-derived reworked deposits in the basin. However, most of our cores in that region did not recover more than a few decimeters of sediment and further drilling is clearly needed to characterize the Anydros basin fill.

In summary, at the present temporal resolution, the hemipelagic sedimentation-rate variations along the Aegean arc do neither show clear correlations with either climate extremes nor with large eruptions, suggesting that local paleomorphological conditions exerted the major control on these rates. Tectonic uplift (Yali) and subsidence (Anydros basin) may have affected sedimentation rates but further work is required to verify that.

7.2. Implications of New Ash-Layer Ages

The ages of the major tephras from Santorini are well constrained and mostly serve as time marker in this study. Therefore, we here focus on the new tephra ages we have obtained for Milos and the Kos-Yali-Nisyros volcanic complex.

The recognition that the Firiplaka Tephra from Milos is widespread demonstrates that plinian eruptions have occurred that were much more powerful than the phreatomagmatic eruptions hitherto recognized on land, and that explosive volcanism on Milos is significantly younger (36.3 ka) than previously thought (>62 ka; Zhou et al., 2021).

The most significant tephra age estimates are those for Nisyros and Yali volcanoes (Figure 11). The Yali-2 eruption appears to have been more complex than implied by the fall deposit on land in that two magma compositions were erupted in such a way that the major, more evolved magma batch formed a widespread marine tephra layer (Yali-2a). The minor, less evolved magma produced a marine tephra layer of limited extent (Yali-2b). Yali-2b, Yali-2a and Yali-1 form a magmatic differentiation trend (Figure 4) but the most evolved Yali-1 magma erupted

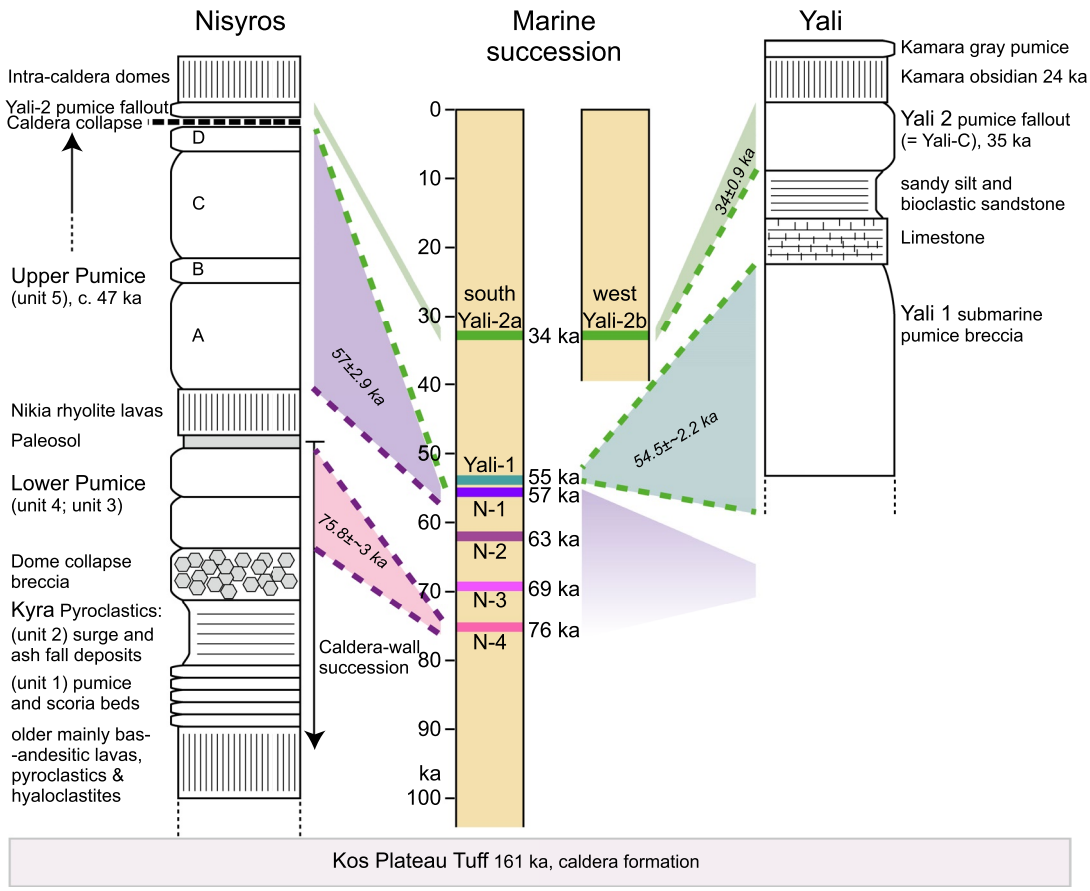

Figure 11. Marine tephrochronology based on the POS 513-53, -52, -50, -45, -44, -43, -35 cores compared with the schematic, not to scale, composite stratigraphic profiles of Nisyros and Yali volcanoes, compiled from Allen and McPhie (2000), Francalanci et al. (1995) and Limburg and Varekamp (1991).

roughly 20 kyrs before the less evolved Yali-2 magma (Figure 12), which appears to have been compositionally zoned. Either the Yali-2 eruption discharged less-evolved magma left after the Yali-1 eruption, or a new, less-evolved magma batch was generated following the Yali-1 eruption. Largely overlapping zircon crystallization ages of Yali-1 and Yali-2 (Popa et al., 2020) probably mostly reflect the age of the underlying mush zone (Bachmann et al., 2012) rather than that of the shallower erupting reservoirs.

The two major eruptions known from Nisyros (Nisyros 1 and Nisyros 4) were separated by a time period of about 20 kyrs during which two other highly explosive, but lower magnitude, eruptions occurred (Figures 11 and 12). The four N-1 through N-4 tephras can be compositionally distinguished from each other but all together form a differentiation trend that is clearly distinct from that formed by the Yali glass compositions (Figures 4, 12; Figure 8 in Part 1). The Nisyros trend could represent progressive differentiation with time probably in a large magma reservoir that was repeatedly tapped without significantly interrupting the differentiation process.

According to Bachmann et al. (2012), the KPT caldera formed by eruption of rhyolitic magma from a large crystal-mush body that was relatively cool and derived from volatile-rich parental melts. A new post-caldera mush zone developed from less volatile-rich parental melts and formed hotter derivative magmas that erupted the Nisyros tephras characterized by higher Zr/Nb and little change in Rb/Sr compared to the KPT-Yali trend, reflecting different onsets of plagioclase and zircon fractionation (Figures 4 and 12). Subsequent lower-temperature and more volatile-rich conditions then produced the Yali-1 composition. Bachmann et al. (2012) apparently did not analyze Yali-2. This model needs to be adjusted in the light of the new age results herein. The Yali-1 submarine eruption may have occurred shortly after (~54.9 ka) the Nisyros-4 caldera-forming eruption on Nisyros (57 ± 2.9 ka) or else, considering the age errors, almost simultaneously. Hence, there was no time between Nisyros-4 and Yali-1 for the entire magma system to change to the new, cooler conditions required to form the highly evolved Yali-1 rhyolite. We therefore suggest that Nisyros and Yali magmas evolved separately such that evolution to

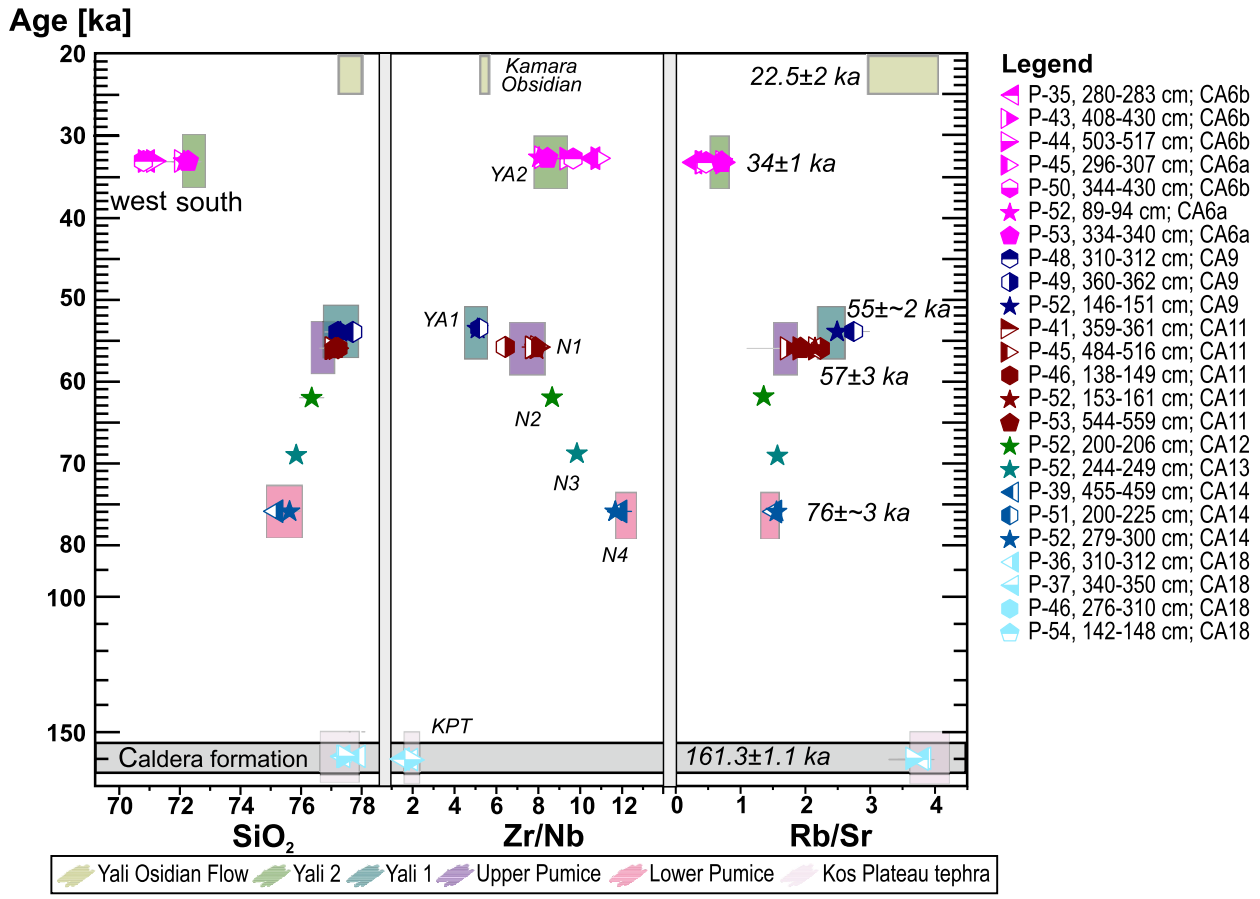

Figure 12. Variations with age of selected geochemical parameters of the glass compositions of the KPT, Nisyros (N1-N4) and Yali tephras (YA1, YA2). Rectangular fields give compositional ranges of samples collected on land, symbols mark glass compositions of marine tephras. Data for Kamara Obsidian from Popa et al. (2019). Terrestrial and marine geochemical data shown are given in the supplementary Tables S2a, S2b, S3a, and S3b of Part 1. Note change of age scale at 80 ka.

Yali-1 magma in the Yali system occurred roughly contemporaneous with the evolution to the Nisyros-4 magma in the Nisyros system. Our new eruption age for Yali-1 suggests that the Yali-1 magma reservoir already existed at the time of the Nisyros-4 eruption.

Our age data also indicate a time gap of ~22 kyrs between the Yali-1 and Yali-2 eruptions, in contrast to only 4.5–7.5 (±10) kyrs implied by the zircon dating of Popa et al. (2020). Based on their earlier (Popa et al., 2019) model of explosive-effusive transition conditions, Popa et al. (2020) concluded that repose times greater than ~12 kyrs at Yali should result in subsequent effusive rather than explosive eruption. This inference may apply to the extrusion of rhyolite lava ~12 kyrs after the Yali-2 eruption (Popa et al., 2020), because the lava bulk-rock and glass compositions are similar to, but differ in detail from, the Yali-1 tephra (Figure 12). For the ~22 kyrs repose between Yali-1 and Yali-2, however, Popa et al. (2020) did not explicitly consider the less evolved magma composition of Yali-2a and Yali-2b with respect to Yali-1 (Figures 4 and 12) which we interpret as a new magma batch after the Yali-1 eruption, as discussed below.

With respect to Yali, our tephra age estimates also have implications for tectonic processes. The proximal Yali-1 tephra, which formed largely under submarine conditions, is covered by carbonate and (bio)clastic sediments that were deposited in very shallow water but now lie at 120 m above sea level (Allen & McPhie, 2000). At the time of the Yali-1 eruption, the sea level was about 50 m lower than today (Figure 9a), implying that an uplift of ~170 m must have occurred since 54 ka, giving an average uplift rate of ~3 mm/yr. This estimate is a minimum because we do not consider the unknown time needed to form the shallow-marine sediments after the Yali-1 eruption. Moreover, uplift above sealevel must already have occurred before 33 ka when Yali-2 tephra erupted subaerially. If all uplift had occurred between 54 to 34 ka, the uplift rate would have been ~8 mm/yr, considering also a few meters sealevel drop between both eruptions, but uplift may have continued after the Yali-2 eruption. Vertical

movements are also evident from several normal faults that offset the Yali-1 tephra by up to 100 m; these offsets must have formed since the Yali-1 emplacement (Allen & McPhie, 2000). Nomikou and Papanikolaou (2011) described a fault zone that extends across Nisyros and Yali, including the Mandraki faults on Nisyros, and that has a 100 m vertical offset on the sea floor between the islands as well as on land. GPS data and earthquakes attest to continued activity on these faults, and the GPS measurements yielded an uplift of up to 30 mm/yr on the Mandraki fault on Nisyros during the 1997–2001 period (Lagios et al., 2005). Long-term average vertical displacements are generally much smaller. For example, subsidence of the eastern margin of the Cyclades plateau between 250 and 18 ka occurred at a mean rate of 0.44 mm/yr (Lykousis, 2009). The mean uplift rate of 0.06 mm/yr over a 3.5 Myr period of Santa Maria volcanic island in the Azores has been attributed to "magmatic thickening" of the thin, young oceanic crust (Ramalho et al., 2017). Over a shorter time period more comparable to the Yali case, Kröchert et al. (2008) determined an uplift of 4 mm/yr during the last 18,000 years for southern Tenerife, Canary Islands. In the absence of compressive tectonics, the high uplift rates of volcanic islands over intermediate (order of 10^4 years) time periods is best explained by magma intrusion. During the phase of active intrusion, the uplift rate would be much higher than the long-term mean rate. For example, the present inflation at Laguna del Maule, Chile, causes >200 mm/yr uplift rate (Le Mével et al., 2021). At such a rate the 170 m uplift at Yali would be achieved within <900 years. From the observation that Yali-2 magma was less evolved than the Yali-1 magma, we suggest that the fast uplift of Yali sometime after the Yali-1 eruption and before the Yali-2 eruption was caused by intrusion of at least ~2 km^3 (Yali-2 erupted magma volume) of less evolved magma into a shallow crustal level (perhaps the ~8 km depth as proposed by Nomikou & Papanikolaou, 2011).

7.3. Implications of Erupted Magma Volumes and Masses

Figure 13 illustrates the temporal sequence of erupted magma volumes at the investigated volcanic complexes. Most of the analyzed tephras (60%) represent eruptions in the eruption magnitude (c.f. Pyle, 2000) range M6 (M5.5 to 6.5), 20% are M7, and the remaining 20% distribute over the M3 to M5 range (Figure 14a). The succession of measured tephras is most complete for Santorini, where the erupted magma volumes add up to a total of 130 km^3 DRE for the last 200 kyrs, which converts to an average magma mass flux of ~40 kg/s (0.65 km^3/ky). These estimates are minimum values because, as stated earlier, they do not include magma masses stored in pyroclastic flow deposits, which are not well constrained but are probably smaller than the fall (plinian and co-ignimbrite) deposit. Also not included are the (unknown) magma masses for the Vourvoulos and other, minor tephras and lavas intercalated between the major tephras (Wulf et al., 2020) but inclusion of these units would not significantly modify the results. For example, the mafic Skaros shield of 12 km^3 (formed between US1 and US2) and the dacitic Therasia dome complex of 2 km^3 (formed between US2 and CT; Fabbro et al., 2013) would together shift the US2 to MT data in Figure 14b to the right by only 0.14×10^{14} kg. Similarly, the volume of 2.2–2.5 km^3 of the pre-Kameni island in the Santorini caldera formed between the Cape Riva and Minoan eruptions (Karátson et al., 2018) adds little to the total erupted magma volume of the Santorini volcanic complex.

The relatively high long-term magma flux of 40 kg/s (slightly lower than ~67 kg/s estimated by Druitt et al., 1999) may have been favored by the extensional tectonic conditions (Nomikou et al., 2016). However, the magma flux varied with time (Figure 14b). Two eruptive cycles have been identified in the Santorini tephra succession (~360 to ~177 ka, and ~177 to 3.6 ka) during which erupted magma compositions became more evolved with time (Druitt et al., 1999). For most of the second cycle (Cape Thera to Cape Tripiti tephras), when erupted magmas had dominantly intermediate compositions, the magma flux remained approximately constant at around 11 kg/s (0.17 km^3/ky; Figure 14b). During the final phase of the cycle (Cape Tripiti to Minoan tephras) when evolved magmas were erupted, the average eruptive magma flux was 196 kg/s (2.7 km^3/ky; Figure 14b). This sharp increase in flux was actually preceded by a minimum flux (~5 kg/s or 0.1 km^3/ky) between US2 and CT (Fabbro et al., 2013). The available data for the first eruptive cycle suggests an average 97 kg/s (1.47 km^3/ky) but data for the Cape Therma 1 and 2 tephras and minor eruptive events are missing.

For the Kos-Yali-Nisyros volcanic complex, the magma masses represented by the major tephras (Figure 13) represent only a fraction of total magma erupted since formation of the KPT caldera, because the intracaldera edifices of Yali and Nisyros and other structures younger than 161 ka (Nomikou et al., 2021) also comprise substantial magma volumes. Nomikou et al. (2021) determined edifice volumes for Nisyros and Yali of 39 km^3, which we estimate to represent ~20 km^3 DRE magma volume. This volume is comparable to the cumulative magma volume of 24 km^3 stored in the major tephras. The edifice magma mass for Nisyros and Yali is $\sim 4.2 \times 10^{13}$ kg

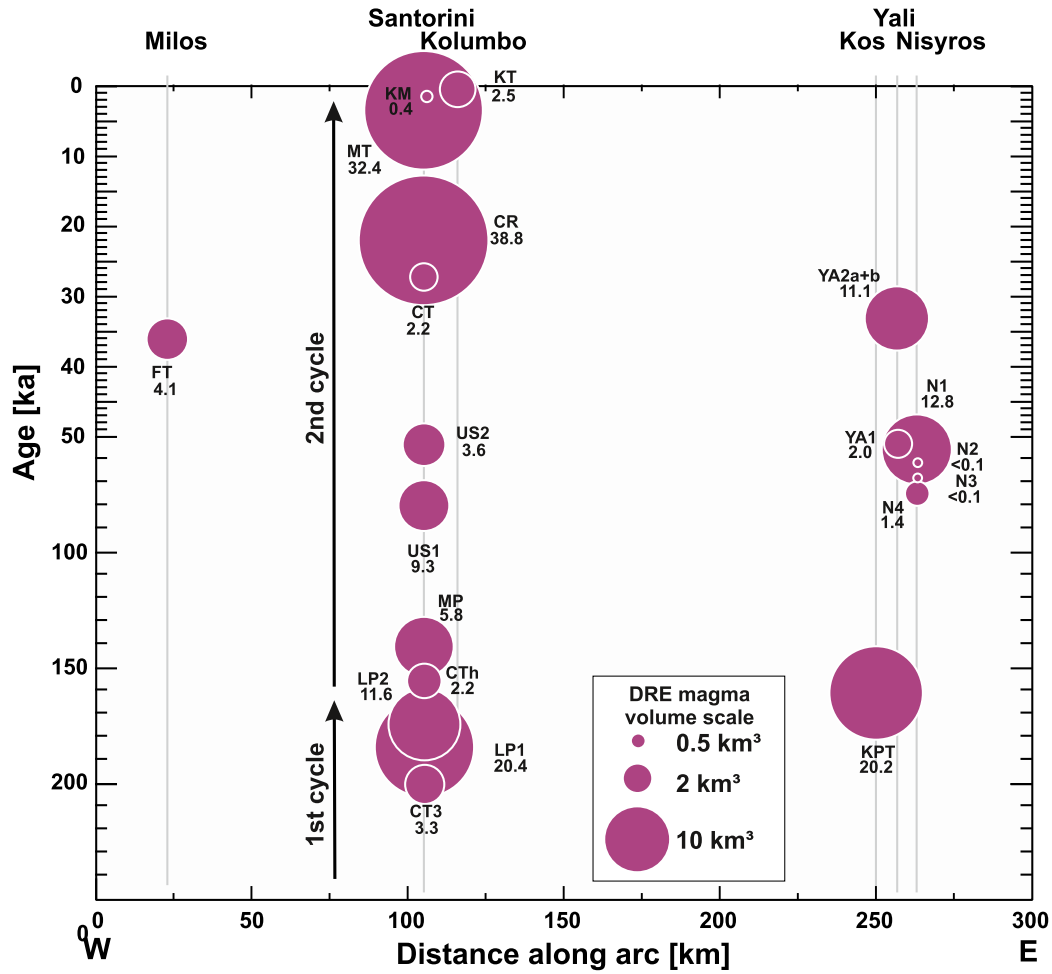

Figure 13. Erupted DRE magma volumes (violet circles, diameters relate to volume-scaled sphere) of tephras from Milos, Santorini – Kolumbo and Kos-Nisyros-Yali arranged by tephra age. Note change of age scale at 50 ka. Distance along the Aegean Volcanic Arc is measured from Antimilos. See Figures 5–7 for tephra acronyms. Numbers next to each circle give the tephra volume in km^3.

and this mass must be added to the KPT mass (dashed line in Figure 14b; the precise timing is not known). The Kos-Yali-Nisyros post-caldera data then show a temporal variation in long-term eruptive magma flux that is similar to the variation observed in the second cycle of Santorini (Figure 14b). The long-term average eruptive mass flux over the 43 kyr period from N4 to Yali-2 is 37 kg/s.

With only one measured tephra each, no temporal variations in erupted magma mass can be constrained for Kolumbo and Milos. The volcanic edifice of Kolumbo, dominantly composed of volcaniclastic deposits, has a volume of 13–22 km^3 within a ~5 km radius which includes the proximal 1650 AD tephra (Hübscher et al., 2015). That edifice volume equals ~9–15 km^3 DRE magma volume and, ignoring the minor proximal overlap, we add 2.9 km^3 DRE of the 1650 AD tephra. This historic explosive eruption discharged 20%–30% of Kolumbo's total magma volume, which is a maximum estimate, because potential distal tephras from older eruption phases contain an unknown additional magma volume. If each of the four pre-1650 phases seismically identified by Hübscher et al. (2015) had magma volumes similar to the 1650 AD tephra, the bulk Kolumbo magma volume could easily be about 12 km^3 larger.

Volcanism on Milos began in the Upper Pliocene and lasted to recent times, forming pyroclastic deposits, lavas and intrusions (Fytikas et al., 1986; Stewart & McPhie, 2006). The island edifice also includes an unknown volume of metamorphic basement (Rinaldi & Campos Venuti, 2003). Thus, it is difficult to place the erupted magma mass contained in the Firiplaka tephra into a context. Stewart and McPhie (2006) stated that the volcanic

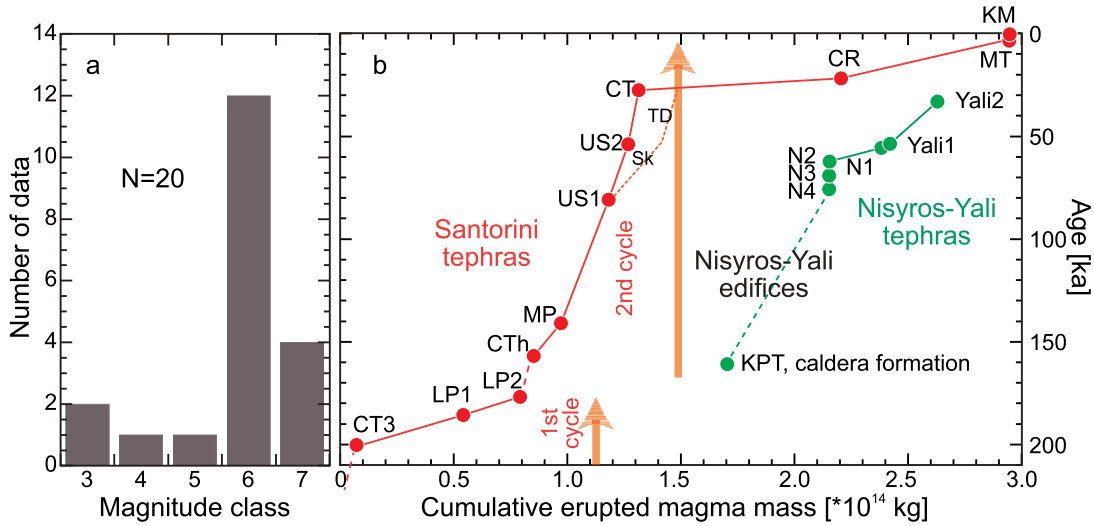

Figure 14. (a) Distribution of analyzed tephras into eruption magnitude (c.f. Mason et al., 2004; Pyle, 2000) bins. Bins are defined as, for example, M6 including all magnitudes $5.5 \leq M < 6.5$. (b) Cumulative erupted magma mass versus age for Santorini and the Kos-Nisyros-Yali volcanic complex. Santorini data ignores minor tephras and lavas emplaced during the last 200 kyrs (cf. Wulf et al., 2020). Orange dotted line indicates how adding the masses of the Skaros shield (Sk) and the Therasia dome complex (TD) would shift younger data slightly to the right. For Kos-Nisyros-Yali, the tephras shown were erupted after the construction of the Nisyros and Yali edifices on the floor of the KPT caldera. The green dashed line indicates the Nisyros-Yali combined edifice volume of ~39 km^3, equivalent to an erupted magma mass of $\sim 4.2 \times 10^{13}$ kg (Nomikou et al., 2021). KM = Kameni, MT = Minoan, CR = Cape Riva, CT = Cape Tripiti, US1 = Upper Scoriae 1, US2 = Upper Scoriae 2, CTh = Cape Thera, MP = Middle Pumice, LP2 = Lower Pumice 2, LP1 = Lower Pumice 1, CT3 = Cape Therma 3, YA1 = Yali 1, YA2 = Yali 2, N1-N4 = Nisyros 1 to 4, KPT = Kos Plateau Tuff.

succession covers an area of 151 km^2 with up to 700 m thickness on the island, which would suggest a bulk edifice volume of 106 km^3, a minimum considering the unknown submarine volume. If, as a rough estimate, the submarine part has 70 km^3 DRE magma volume, then the widespread Firiplaka tephra (4 km^3 DRE) would account for almost 6% of the magma mass that may have been emplaced in the past 3 Myrs (Fytikas et al., 1986). More and deeper marine sediment cores are needed to test if such a large-magnitude eruption ($M = 5.9$) was very unusual for Milos or occurred more frequently in the past.

8. Conclusions

Using time marks provided by dated marine tephras, we have determined apparent hemipelagic sedimentation rates for the Aegean Sea between the islands of Milos in the west and Nisyros in the east. Some of these data reach back to ~160 ka but most are <80 ka. We have discussed these data in the context of large sealevel and coastline changes, source material provision by large explosive eruptions, and paleomorphologic position as well as relation to tectonic uplift and subsidence.

We have determined the ages of seven previously undated tephras using the sedimentation rate at the respective core intervals. Most of these ages are well constrained by measurements in several cores. The seven new ages are 37.0 ± 1.3 ka for the Firiplaka Tephra from Milos, 34.0 ± 0.9 ka for Yali 2 fall deposit (which roughly agrees with the 31 ka age based on oxygen isotope stratigraphy; Federman & Carey, 1980), ~54.9 ka for the Yali 1 pumice breccia, 57.0 ± 2.9 ka for the marine Nisyros 1 tephra, equivalent to Upper Pumice on Nisyros, ~63.1 ka and ~68.9 ka for Nisyros 2 and Nisyros 3 marine tephras not yet found on land, and ~75.8 ka for Nisyros 4, equivalent to the Lower Pumice on Nisyros.

The 37.0 ± 1.3 ka age of the Firiplaka Tephra has important implications for volcanic hazard assessment at Milos because it shows that highly explosive volcanism extended to much younger times than those suggested by radiometric dating (>60 ka; Zhou et al., 2021), in addition to showing that plinian eruptions have occurred that have not yet been recognized in the onshore stratigraphy.

The Yali and Nisyros tephra ages resolve long-standing age data conflicts for the post-caldera Kos-Nisyros-Yali volcanism. The different petrological characteristics of the Nisyros and Yali volcanic rocks have been interpreted

as a temporal change in fractionation paths within a large crustal magma reservoir governed by input from depth of magmas changing from lower to higher volatile contents (Bachmann et al., 2012; Francalanci et al., 1995). The almost contemporaneous eruption of the Upper Pumice from Nisyros and the Yali-1 pumice breccia leaves no time for a gradual change but implies coexistence of two petrologically different magma reservoirs at Nisyros and Yali despite their close proximity.

Isopach maps of 20 tephras have been constructed; 15 are well constrained by numerous thickness data but 5 are based on limited data. Tephra volumes, magma volumes and magma masses have been determined, based on these maps. In the case of Santorini, these data cover almost the complete succession of major tephras known on land, and add up to a total magma DRE volume of at least 130 km^3. The long-term average eruptive mass flux during the last 200 kyr on Santorini is ~40 kg/s but magma flux varied temporally from values as low as 5 kg/s during periods of intermediate magma eruptions and dacitic dome extrusion to values as high as 160 kg/s during periods of highly explosive eruptions of the most evolved magmas. Applying the same approach to Kos-Nisyros-Yali post-caldera volcanism suggests a similar average rate of ~37 kg/s but is less well constrained because little is known about the volcanism between 161 ka (Kos Plateau Tuff caldera formation) and 76 ka (Lower Pumice from Nisyros) in that area.

Data Availability Statement

All data produced during this study is under way at Kutterolf, Freundt, Druitt, et al. (2021) in PANGAEA Data Archiving and Publication (https://doi.org/10.1594/PANGAEA.937928). An electronic copy of this data file is provided as Tables S1–S3 in Data Set S1.

Acknowledgments
The RV POSEIDON cruise POS 513 in 2017 and the subsequent analytical work were financed by GEOMAR Helmholtz Centre for Ocean Research Kiel. We would like to thank R. Dettbarn, F. Hampel, C. Sievers, C. Wittig, K.-L. Wang, and H.-Y. Lee for their contributions to our reference data base. This is Laboratory of Excellence ClerVolc Contribution Number 503. We gratefully acknowledge constructive reviews by Ralf Gertisser, Sabine Wulf and an anonymous reviewer.

References

Aksu, A. E., Jenner, G., Hiscott, R. N., & Isler, E. B. (2008). Occurrence, stratigraphy and geochemistry of Late Quaternary tephra layers in the Aegean Sea and the Marmara Sea. *Marine Geology*, *252*, 174–192. https://doi.org/10.1016/j.margeo.2008.04.004

Albert, P. G., Hardiman, M., Keller, J., Tomlinson, E. L., Smith, V. C., Bourne, A. J., et al. (2015). Revisiting the Y-3 tephrostratigraphic marker: A new diagnostic glass geochemistry, age estimate, and details on its climatostratigraphical context. *Quaternary Science Reviews*, *118*, 105–121. https://doi.org/10.1016/j.quascirev.2014.04.002

Allen, S. R., & Cas, R. A. F. (1998). Rhyolitic fallout and pyroclastic density current deposits from a phreatoplinian eruption in the eastern Aegean Sea, Greece. *Journal of Volcanology and Geothermal Research*, *86*, 219–251. https://doi.org/10.1016/s0377-0273(98)00080-8

Allen, S. R., & Cas, R. A. F. (2001). Transport of pyroclastic flows across the sea during the explosive, rhyolitic eruption of the Kos Plateau Tuff, Greece. *Bulletin of Volcanology*, *62*, 441–456. https://doi.org/10.1007/s004450000107

Allen, S. R., & McPhie, J. (2000). Water-settling and resedimentation of submarine rhyolitic pumice at Yali, eastern Aegean, Greece. *Journal of Volcanology and Geothermal Research*, *95*, 285–307. https://doi.org/10.1016/s0377-0273(99)00127-4

Allen, S. R., Stadlbauer, E., & Keller, J. (1999). Stratigraphy of the Kos Plateau Tuff: Product of a major Quaternary explosive rhyolitic eruption in the eastern Aegean, Greece. *International Journal of Earth Science*, *88*, 132–156. https://doi.org/10.1007/s005310050251

Anagnostopoulos, V. K., & Anastasakis, G. (2021). Volcanogenic mass flow deposits and seafloor diapirism following the largest insular Quaternary eruption of the eastern Mediterranean at Nisyros island, Aegean volcanic arc. *Marine Geology*, *425*(2020), 106185. https://doi.org/10.1016/j.margeo.2020.106185

Bachmann, O., Deering, C. D., Ruprecht, J. S., Huber, C., Skopelitis, A., & Schnyder, C. (2012). Evolution of silicic magmas in the Kos-Nisyros volcanic center, Greece: Cycles associated with caldera collapse. *Contributions to Mineralogy and Petrology*, *163*, 155–166. https://doi.org/10.1007/s00410-011-0663-y

Bachmann, O., Schoene, B., Schnyder, C., & Spikings, R. (2010). The Ar-40/Ar-39 and U/Pb dating of young rhyolites in the Kos-Nisyros volcanic complex, Eastern Aegean Arc, Greece: Age discordance due to excess Ar-40 in biotite. *Geochemistry, Geophysics, Geosystems*, *11*, Q0AA08. https://doi.org/10.1029/2010gc003073

Benjamin, J., Rovere, A., Fontana, A., Furlani, S., Vacchi, M., Inglis, R. H., et al. (2017). Late Quaternary sea-level changes and early human societies in the central and eastern Mediterranean Basin: An interdisciplinary review. *Quaternary International*, *449*, 29–57. https://doi.org/10.1016/j.quaint.2017.06.025

Bonadonna, C., & Costa, A. (2012). Estimating the volume of tephra deposits: A new simple strategy. *Geology*, *40*(5), 415–418. https://doi.org/10.1130/g32769.1

Bonadonna, C., & Costa, A. (2013). Plume height, volume, and classification of explosive volcanic eruptions based on the Weibull function. *Bulletin of Volcanology*, *75*(8), 742. https://doi.org/10.1007/s00445-013-0742-1

Bonneau, M., & Kienast, J. R. (1982). Subduction, collision et schistes bleus: Exemple de l'Egée. *Bulletin De La Societe Geologique De France*, *7*, 785–791. https://doi.org/10.2113/gssgfbull.s7-xxiv.4.785

Boyce, J. A., & Gertisser, R. (2012). Variations in welding characteristics within the Plinian air-fall deposit of the Middle Pumice eruption, Santorini, Greece. *Journal of Volcanology and Geothermal Research*, *221–222*, 71–82. https://doi.org/10.1016/j.jvolgeores.2012.01.004

Bronk Ramsey, C., Albert, P. G., Blockley, S. P. E., Hardiman, M., Houley, R. A., Lane, C. S., et al. (2015). Improved age estimates for key Late Quaternary European tephra horizons in the RESET lattice. *Quaternary Science Reviews*, *118*, 18–32. https://doi.org/10.1016/j.quascirev.2014.11.007

Bronk Ramsey, C., Housley, R. A., Lane, C. S., Smith, V. C., & Pollard, A. M. (2015). The RESET tephra database and associated analytical tools. *Quaternary Science Reviews*, *118*, 33–47. https://doi.org/10.1016/j.quascirev.2014.11.008

Campos Venuti, M., & Rossi, R. L. (1996). Depositional facies in the Firiplaka rhyolitic Tuff Ring, Milos Island (Cyclades, Greece). *Acta Vulcanologica*, *8*(2), 47–63.

Cane, T., Rohling, E. J., Kemp, A. E. S., Cooke, S., & Pearce, R. B. (2002). High-resolution stratigraphic framework for Mediterranean sapropel S5: Defining temporal relationships between records of Eemian climate variability. *Palaeogeography, Palaeoclimatology, Palaeoecology*, *183*, 87–101. https://doi.org/10.1016/s0031-0182(01)00461-8

Cantner, K., Carey, S., & Nomikou, P. (2014). Integrated volcanologic and petrologic analysis of the 1650 AD eruption of Kolumbo submarine volcano, Greece. *Journal of Volcanology and Geothermal Research*, *269*, 28–43. https://doi.org/10.1016/j.jvolgeores.2013.10.004

Cullen, V. L., Smith, V. C., & Arz, H. W. (2014). The detailed tephrostratigraphy of a core from the south-east Black sea spanning the last ~60 ka. *Journal of Quaternary Science*, *29*(7), 675–690. https://doi.org/10.1002/jqs.2739

Dietrich, V. J., & Lagios, E. (2018). Nisyros Volcano. The Kos-Yali-Nisyros volcanic field *Active volcanoes of the world* (Vol. XII, p. 339).

Druitt, T. H. (1985). Vent evolution and lag breccia formation during the Cape Riva eruption of Santorini, Greece. *The Journal of Geology*, *93*, 439–454. https://doi.org/10.1086/628965

Druitt, T. H. (2014). New insights into the initiation and venting of the Bronze-Age eruption of Santorini (Greece), from component analysis. *Bulletin of Volcanology*, *76*, 794. https://doi.org/10.1007/s00445-014-0794-x

Druitt, T. H., Edwards, L., Mellors, R. A., Pyle, D. M., Sparks, R. S. J., Lanphere, M., et al. (1999). Santorini volcano. *Geological Society, London, Memoirs*, *19*, 165.

Druitt, T. H., & Francaviglia, V. (1992). Caldera formation on Santorini and the physiography of the islands in the late Bronze Age. *Bulletin of Volcanology*, *54*, 484–493. https://doi.org/10.1007/bf00301394

Druitt, T. H., Mellors, R. A., Pyle, D. M., & Sparks, R. S. J. (1989). Explosive volcanism on Santorini, Greece. *Geological Magazine*, *126*, 95–126. https://doi.org/10.1017/s0016756800006270

Druitt, T. H., Mercier, M., Florentin, L., Deloule, E., Cluzel, N., Flaherty, T., et al. (2016). Magma storage and extraction associated with plinian and interplinian activity at Santorini caldera (Greece). *Journal of Petrology*, *57*, 461–494. https://doi.org/10.1093/petrology/egw015

Druitt, T. H., & Sparks, R. S. J. (1982). A proximal ignimbrite breccia facies on Santorini, Greece. *Journal of Volcanology and Geothermal Research*, *13*, 147–171. https://doi.org/10.1016/0377-0273(82)90025-7

Eastwood, W. J., Pearce, N. J. G., Westgate, J. A., Perkins, W. T., Lamb, H. F., & Roberts, N. (1999). Geochemistry of Santorini tephra in lake sediments from Southwest Turkey. *Global and Planetary Change*, *21*, 17–29. https://doi.org/10.1016/s0921-8181(99)00005-3

Fabbro, G. N., Druitt, T. H., & Scaillet, S. (2013). Evolution of the crustal magma plumbing system during the build-up to the 22-ka caldera-forming eruption of Santorini (Greece). *Bulletin of Volcanology*, *75*, 767. https://doi.org/10.1007/s00445-013-0767-5

Federman, A. N., & Carey, S. N. (1980). Electron microprobe correlation of tephras from eastern Mediterranean abyssal sediments and the island of Santorini. *Quaternary Research*, *13*, 160–171. https://doi.org/10.1016/0033-5894(80)90026-5

Fierstein, J., & Nathenson, M. (1992). Another look at the calculation of fallout tephra volumes. *Bulletin of Volcanology*, *54*, 156–167. https://doi.org/10.1007/bf00278005

Filippidi, A., Triantaphyllou, M. V., & De Lange, G. J. (2016). Eastern-Mediterranean ventilation variability during sapropel S1 formation, evaluated at two sites influenced by deep-water formation from Adriatic and Aegean Seas. *Quaternary Science Reviews*, *144*, 95–106. https://doi.org/10.1016/j.quascirev.2016.05.024

Francalanci, L., Varekamp, J. C., Vougioukalaskis, G., Defant, M. J., Innocenti, F., & Manetti, P. (1995). Crystal retention, fractionation and crustal assimilation in a convecting magma chamber, Nisyros Volcano, Greece. *Bulletin of Volcanology*, *56*, 601–620. https://doi.org/10.1007/bf00301465

Francalanci, L., Vougioukalakis, G. E., Perini, G., & Manetti, P. (2005). A west-east traverse along the magmatism of the south Aegean volcanic arc in the light of volcanological, chemical and isotopic data. In M. Fytikas, & G. E. Vougioukalakis (Eds.), *The south Aegean active volcanic arc* (pp. 64–112). Elsevier.

Friedrich, W. L., Kromer, B., Friedrich, M., Heinemeier, J., Pfeiffer, T., & Talamo, S. (2006). Santorini eruption radiocarbon dated to 1627-1600 B.C. *Science*, *312*(5773), 548–548. https://doi.org/10.1126/science.1125087

Freundt, A. (2017). *POS 513 cruise report* (p. 18). GEOMAR. https://doi.org/10.3289/cr_pos513

Freundt, A., Schindlbeck-Belo, J. C., Kutterolf, S., & Hopkins, J. L. (2021). Tephra layers in the marine environment: A review of properties and emplacement processes. *Geological Society, London, Special Publications*, *520*. https://doi.org/10.1144/SP520-2021-50

Fuller, S., Carey, S., & Nomikou, P. (2018). Distribution of fine-grained tephra from the 1650 CE submarine eruption of Kolumbo. *Journal of Volcanology and Geothermal Research*, *352*, 10–25. https://doi.org/10.1016/j.jvolgeores.2018.01.004

Fytikas, M., Innocenti, F., Kolios, N., Manetti, P., Mazzuoli, R., Poli, G., et al. (1986). Volcanology and petrology of volcanic products from the island of Milos and neighbouring islets. *Journal of Volcanology and Geothermal Research*, *28*, 297–317. https://doi.org/10.1016/0377-0273(86)90028-4

Gertisser, R., Preece, K., & Keller, J. (2009). The Plinian Lower Pumice 2 eruption, Santorini, Greece: Magma evolution and volatile behaviour. *Journal of Volcanology and Geothermal Research*, *186*, 387–406. https://doi.org/10.1016/j.jvolgeores.2009.07.015

Giaccio, B., Hajdas, I., Isaia, R., Deino, A., & Nomade, S. (2017). High-precision ^{14}C and $^{40}Ar/^{39}Ar$ dating of the Campanian Ignimbrite (Y-5) reconciles the time-scales of climatic-cultural processes at 40 ka. *Scientific Reports*, *7*, 45940. https://doi.org/10.1038/srep45940

Grant, K. M., Rohling, E. J., Westerhold, T., Zabel, M., Heslop, D., Konijnendijk, T., & Lourens, L. (2017). A 3 million year index for North African humidity/aridity and the implication of potential pan-African Humid periods. *Quaternary Science Reviews*, *171*, 100–118. https://doi.org/10.1016/j.quascirev.2017.07.005

Green, M. G., Bebbington, M. S., Jones, G., Cronin, S. J., & Turner, M. B. (2016). Estimation of tephra volumes from sparse and incompletely observed deposit thicknesses. *Bulletin of Volcanology*, *78*. https://doi.org/10.1007/s00445-016-1016-5

Hardiman, J. C. (1999). Deep sea tephra from Nisyros Island, eastern Aegean Sea, Greece. In C. R. Firth, & W. J. McGuire (Eds.), *Volcanoes in the quaternary* (Vol. 161, pp. 69–88). Geological Society, London, Special Publications. https://doi.org/10.1144/gsl.sp.1999.161.01.06

Houghton, B. F., Wilson, C. J. N., & Pyle, D. M. (2000). Pyroclastic fall deposits. In H. Sigurdsson (Ed.), *Encyclopedia of volcanoes* (pp. 555–570). Academic Press.

Hübscher, C., Ruhnau, M., & Nomikou, P. (2015). Volcano-tectonic evolution of the polygenetic Kolumbo submarine volcano/Santorini (Aegean Sea). *Journal of Volcanology and Geothermal Research*, *291*, 101–111.

Isler, E. B., Aksu, A. E., & Hiscott, R. N. (2016). Geochemistry of Aegean Sea sediments: Implications for surface- and bottom-water conditions during sapropel deposition since MIS 5. *Turkish Journal of Earth Sciences*, *25*, 103–125.

Karátson, D., Gertisser, R., Telbisz, T., Vereb, V., Quidelleur, X., Druitt, T., et al. (2018). Towards reconstruction of the lost Late Bronze Age intra-caldera island of Santorini, Greece. *Scientific Reports*, *8*, 7026. https://doi.org/10.1038/s41598-018-25301-2

Karkanas, P., White, D., Lane, C. S., Stringer, C., Davies, W., Cullen, V. L., et al. (2015). Tephra correlations and climatic events between the MIS6/5 transition and the beginning of MIS3 in Theopetra Cave, central Greece. *Quaternary Science Reviews*, *118*, 170–181. https://doi.org/10.1016/j.quascirev.2014.05.027

Karstens, J., Crutchley, G., Elger, J., Kühn, M., Schmid, F., Dalla Valle, G., et al. (2020). *R/V Poseidon cruise report 538 - THESEUS Tsunami hazard of explosive submarine eruptions, 7th October – 28th October 2019, Cartagena (Spain) - Heraklion (Greece)* (pp. 106). GEOMAR Helmholtz Centre for Ocean Research. https://doi.org/10.3289/cr_pos538

Keller, J., Gertisser, R., Reusser, E., & Dietrich, V. (2014). Pumice deposits of the Santorini Lower Pumice 2 eruption on Anafi island, Greece: Indications for a Plinian event of exceptional magnitude. *Journal of Volcanology and Geothermal Research*, *278–279*, 120–128. https://doi.org/10.1016/j.jvolgeores.2014.04.009

Keller, J., Ryan, W. B. F., Ninkovich, D., & Altherr, R. (1978). Explosive volcanic activity in the Mediterranean over the past 200.000 years as recorded in deep-sea sediments. *The Geological Society of America Bulletin*, *89*, 591–604. https://doi.org/10.1130/0016-7606(1978)89<591:evaitm>2.0.co;2

Kinvig, H. S., Winson, A., & Gottsmann, J. (2010). Analysis of volcanic threat from Nisyros Island, Greece, with implications for aviation and population exposure. *Natural Hazards and Earth System Sciences*, *10*, 1101–1113. https://doi.org/10.5194/nhess-10-1101-2010

Klawonn, M., Houghton, B. F., Swanson, D. A., Fagents, S. A., Wessel, P., & Wolfe, C. J. (2014). Constraining explosive volcanism: Subjective choices during estimates of eruption magnitude. *Bulletin of Volcanology*, *76*. https://doi.org/10.1007/s00445-013-0793-3

Kröchert, J., Maurer, H., & Buchner, E. (2008). Fossil beaches as evidence for significant uplift of Tenerife, Canary Islands. *Journal of African Earth Sciences*, *51*, 220–234. https://doi.org/10.1016/j.jafrearsci.2008.01.005

Kroon, D., Alexander, I., Little, M., Lourens, L. J., Matthewson, A., Robertson, A. H. F., & Sakamoto, T. (1998). Oxygen isotope and sapropel stratigraphy in the eastern Mediterranean during the last 3.2 million years. In A. H. F. Robertson, K. C. Emeis, C. Richter, & A. Camerlenghi (Eds.), *Proceedings ODP sci res* (Vol. 160, pp. 181–189). https://doi.org/10.2973/odp.proc.sr.160.071.1998

Kutterolf, S., Freundt, A., Druitt, T. H., McPhie, J., Nomikou, P., Pank, K., et al. (2021). Marine tephra thicknesses, density measurements, sedimentation rates and ages of Aegean Arc tephras. *PANGAEA*. https://doi.org/10.1594/PANGAEA.938615.

Kutterolf, S., Freundt, A., Hansteen, T. H., Dettbarn, R., Hampel, F., Sievers, C., et al. (2021). The medial offshore record of explosive volcanism along the Central to Eastern Aegean Arc, part 1: Tephrostratigraphic correlations. *Geochemistry, Geophysics, Geosystems*. https://doi.org/10.1029/2021GC010010

Kutterolf, S., Freundt, A., & Peréz, W. (2008). Pacific offshore record of plinian arc volcanism in Central America: 2. Tephra volumes and erupted masses. *Geochemistry, Geophysics, Geosystems*, *9*, Q02S02. https://doi.org/10.1029/2007GC001791

Kutterolf, S., Freundt, A., Peréz, W., Mörz, T., Schacht, U., Wehrmann, H., & Schmincke, H. U. (2008). Pacific offshore record of plinian arc volcanism in Central America: 1. Along-arc correlations. *Geochemistry, Geophysics, Geosystems*, *9*, Q02S01. https://doi.org/10.1029/2007GC001631

Kutterolf, S., Freundt, A., Pérez, W., Wehrmann, H., & Schmincke, H. U. (2007). Late Pleistocene to Holocene temporal succession and magnitudes of highly-explosive volcanic eruptions in west-central Nicaragua. *Journal of Volcanology and Geothermal Research*, *163*, 55–82. https://doi.org/10.1016/j.jvolgeores.2007.02.006

Kutterolf, S., Freundt, A., Schacht, U., Bürk, D., Harders, R., Mörz, T., & Peréz, W. (2008). Pacific offshore record of plinian arc volcanism in Central America: 3. Application to forearc geology. *Geochemistry, Geophysics, Geosystems*, *9*, Q02S03. https://doi.org/10.1029/2007GC001826

Kutterolf, S., Jegen, M., Mitrovica, J. X., Kwasnitschka, T., Freundt, A., & Huybers, P. (2013). A detection of Milankovitch frequencies in global volcanic activity. *Geology*, *41*(2), 227–230. https://doi.org/10.1130/G33419.1

Kutterolf, S., Schindlbeck, J. C., Anselmetti, F. S., Ariztegui, D., Brenner, M., Curtis, J. H., et al. (2016). A 400-ka tephrochronological framework for Central America from Lake Petén Itzá (Guatemala) sediments. *Quarternary Science Reviews*, *150*, 200–220. https://doi.org/10.1016/j.quascirev.2016.08.023

Kwiecien, O., Arz, H. W., Lamy, F., Wulf, S., Bahr, A., Röhl, U., & Haug, G. H. (2008). Estimated reservoir ages of the Black Sea since the Last Glacial. *Radiocarbon*, *50*(1), 1–20. https://doi.org/10.1017/s0033822200043393

Lagios, E., Sakkas, V., Parcharidis, I., & Dietrich, V. (2005). Ground deformation of Nisyros Volcano (Greece) for the period 1995–2002: Results from DInSAR and DGPS observations. *Bulletin of Volcanology*, *68*, 201–214. https://doi.org/10.1007/s00445-005-0004-y

Legros, F. (2000). Minimum volume of a tephra fallout deposit estimated from a single isopach. *Journal of Volcanology and Geothermal Research*, *96*(1), 25–32. https://doi.org/10.1016/s0377-0273(99)00135-3

Le Mével, H., Córdova, L., Cardona, C., & Feigl, K. L. (2021). Unrest at the Laguna del Maule volcanic field 2005–2020: Renewed acceleration of deformation. *Bulletin of Volcanology*, *83*, 39. https://doi.org/10.1007/s00445-021-01457-0

Limburg, E. M., & Varekamp, C. (1991). Young Pumice deposits on Nisyros, Greece. *Bulletin of Volcanology*, *54*, 68–77. https://doi.org/10.1007/bf00278207

Livanos, I., Nomikou, P., Papanikolaou, D., & Rousakis, G. (2013). Volcanic Debris Avalanche at the SE submarine slopes of Nisyros Volcano, Greece. *Geo-Marine Letters*, *33*, 419–431. https://doi.org/10.1007/s00367-013-0338-y

Lykousis, V. (2009). Sea-level changes and shelf break prograding sequences during the last 400 ka in the Aegean margins: Subsidence rates and palaeogeographic implications. *Continental Shelf Research*, *29*(16), 2037–2044. https://doi.org/10.1016/j.csr.2008.11.005

Makris, J., Papoulia, J., & Yegorova, T. (2013). A 3-D density model of Greece constrained by gravity and seismic data. *Geophysical Journal International*, *194*, 1–17. https://doi.org/10.1093/gji/ggt059

Margari, V., Pyle, D. M., Bryant, C., & Gibbard, P. L. (2007). Mediterranean tephra stratigraphy revisited: Results from a long terrestrial sequence on Lesvos Island, Greece. *Journal of Volcanology and Geothermal Research*, *163*, 34–54. https://doi.org/10.1016/j.jvolgeores.2007.02.002

Mason, B. G., Pyle, D. M., & Oppenheimer, C. (2004). The size and frequency of the largest explosive eruptions on Earth. *Bulletin of Volcanology*, *66*, 735–748. https://doi.org/10.1007/s00445-004-0355-9

McCoy, F. W. (1981). Areal distribution, redeposition and mixing of tephra within deep-sea sediments of the Eastern Mediterranean sea. In S. Self, & R. S. J. Sparks (Eds.), *Tephra studies. Nato advanced study institutes series C 75* (pp. 245–254). Reidel. https://doi.org/10.1007/978-94-009-8537-7_15

McKenzie, D. P. (1972). Active tectonics of the Mediterranean region. *Geophysical Journal of the Royal Astronomical Society*, *30*, 109–185. https://doi.org/10.1111/j.1365-246x.1972.tb02351.x

Mellors, R. A., & Sparks, R. S. J. (1991). Spatter-rich pyroclastic flow deposits on Santorini, Greece. *Bulletin of Volcanology*, *53*, 327–342. https://doi.org/10.1007/BF00280225

Narcisi, B., & Vezzoli, L. (1999). Quaternary stratigraphy of distal tephra layers in the Mediterranean—An overview. *Global and Planetary Change*, *21*, 31–50. https://doi.org/10.1016/s0921-8181(99)00006-5

Nomikou, P., Croff Bell, K. L., Papanikolaou, D., Livanos, I., & Martin, J. F. (2013). Exploring the Avyssos-Yali-Strongyli submarine volcanic complex at the eastern edge of the Aegean volcanic arc. *Zeitschrift für Geomorphologie*, *57*, 127–137. https://doi.org/10.1127/0372-8854/2013/s-00147

Nomikou, P., Huebscher, C., Ruhnau, M., & Bejelou, K. (2016). Tectono-stratigraphic evolution through successive extensional events of the Anydros Basin, hosting Kolumbo volcanic field at the Aegean Sea, Greece. *Tectonophysics*, *671*, 202–217. https://doi.org/10.1016/j.tecto.2016.01.021

Nomikou, P., Krassakis, P., Kazana, S., Papanikolaou, D., & Koukouzas, N. (2021). The volcanic relief within the Kos-Nisyros-Tilos tectonic graben at the eastern edge of the Aegean volcanic arc, Greece and geohazard implications. *Geosciences*, *11*, 231. https://doi.org/10.3390/geosciences11060231

Nomikou, P., & Papanikolaou, D. (2011). Extension of active fault zones on Nisyros volcano across the Yali-Nisyros Channel based on onshore and offshore data. *Marine Geophysical Researches*, *32*, 181–192. https://doi.org/10.1007/s11001-011-9119-z

Nomikou, P., Papanikolaou, D., Alexandri, M., Sakellariou, D., & Rousakis, G. (2013). Submarine volcanoes along the Aegean volcanic arc. *Tectonophysics*, *597–598*, 123–146. https://doi.org/10.1016/j.tecto.2012.10.001

Papazachos, B. C., Dimitriadis, S. T., Panagiotopoulos, D. G., Papazachos, C. B., & Papadimitriou, E. E. (2005). Deep structure and active tectonics of the southern Aegean volcanic arc. In M. Fytikas, & G. E. Vougioukalakis (Eds.), *The South Aegean active volcanic arc* (pp. 4–64). Elsevier. https://doi.org/10.1016/s1871-644x(05)80032-4

Paterne, M., Labeyrie, J., Guichard, F., Mazaud, A., & Maitre, F. (1990). Fluctuations of the Campanian explosive volcanic activity (south Italy) during the past 190 000 years as determined by marine tephrochronology. *Earth and Planetary Science Letters*, *98*, 166–174. https://doi.org/10.1016/0012-821x(90)90057-5

Pe-Piper, G., & Piper, D. J. W. (2005). The South Aegean active volcanic arc: Relationships between magmatism and tectonics. *Developments in Volcanology*, *7*, 113–133. https://doi.org/10.1016/s1871-644x(05)80034-8

Popa, R.-G., Bachmann, O., Ellis, B. S., Degruyter, W., Tollan, P., & Kyriakopoulos, K. (2019). A connection between magma chamber processes and eruptive styles revealed at Nisyros-Yali volcano (Greece). *Journal of Volcanology and Geothermal Research*, *387*, 106666. https://doi.org/10.1016/j.jvolgeores.2019.106666

Popa, R.-G., Guillong, M., Bachmann, O., Szymanowski, D., & Ellis, B. (2020). U-Th zircon dating reveals a correlation between eruptive styles and repose periods at the Nisyros-Yali volcanic area, Greece. *Chemical Geology*, *555*, 119830. https://doi.org/10.1016/j.chemgeo.2020.119830

Pyle, D. M. (1989). The thickness, volume and grain size of tephra fall deposits. *Bulletin of Volcanology*, *51*, 1–15. https://doi.org/10.1007/bf01086757

Pyle, D. M. (2000). Sizes of volcanic eruptions. In H. Sigurdsson et al. (Eds.), *Encyclopedia of volcanoes* (pp. 263–269). Academic Press.

Pyle, D. M., & Margari, V. (2009). Reply: Correlation of a widespread Pleistocene tephra marker from the Nisyros–Yali volcanic complex, Greece. *Journal of Volcanology and Geothermal Research*, *181*, 251–254. https://doi.org/10.1016/j.jvolgeores.2008.11.033

Railsback, L. B., Gibbard, P. L., Head, M. J., Voarintsoa, N. R. G., & Toucanne, S. (2015). An optimized scheme of lettered marine isotope substages for the last 1.0 million years, and the climatostratigraphic nature of isotope stages and substages. *Quaternary Science Reviews*, *111*, 94–106. https://doi.org/10.1016/j.quascirev.2015.01.012

Ramalho, R. S., Helffrich, G., Madeira, J., Cosca, M., Thomas, C., Quartau, R., et al. (2017). Emergence and evolution of Santa Maria Island (Azores)—The conundrum of uplifted islands revisited. *GSA Bulletin*, *129*(3/4), 372–390. https://doi.org/10.1130/B31538.1

Rehren, T. (1988). *Geochemie und Petrologie von Nisyros (Ofstliche Agais)*. Ph.D thesis. Department of Geology, University of Freiburg.

Rinaldi, M., & Campos Venuti, M. (2003). The submarine eruption of the Bombarda volcano, Milos Island, Cyclades, Greece. *Bulletin of Volcanology*, *65*, 282–293. https://doi.org/10.1007/s00445-002-0260-z

Roeser, P. A., Franz, S. O., Litt, t., Ülgen, U. B., Hilgers, A., Wulf, S., et al. (2012). Lithostratigraphic and geochronological framework for the paleoenvironmental reconstruction of the last ~36 ka cal BP from a sediment record from Lake Iznik (NW Turkey). *Quaternary International*, *274*, 73–87. https://doi.org/10.1016/j.quaint.2012.06.006

Rohling, E. J., Marino, G., & Grant, K. M. (2015). Mediterranean climate and oceanography, and the periodic development of anoxic events (sapropels). *Earth-Science Reviews*, *143*, 62–97. https://doi.org/10.1016/j.earscirev.2015.01.008

Ryan, W. B. F., Carbotte, S. M., Coplan, J. O., O'Hara, S., Melkonian, A., Arko, R., et al. (2009). Global multi-resolution topography synthesis. *Geochemistry, Geophysics, Geosystems*, *10*, Q03014. https://doi.org/10.1029/2008GC002332

Sakellariou, D., & Galanidou, N. (2016). Pleistocene submerged landscapes and Palaeolithic archaeology in the tectonically active Aegean region. In J. Harff, G. Bailey, & F. Lüth (Eds.), *Geology and archaeology: Submerged landscapes of the continental shelf* (Vol. 411, pp. 145–178). Geological Society, London, Special Publications. https://doi.org/10.1144/sp411.9

Sakellariou, D., & Galanidou, N. (2017). Aegean Pleistocene landscapes above and below sea level: Palaeogeographic reconstruction and hominin dispersals. Chapter 22. In G. N. Bailey, J. Harff, & D. Sakellariou (Eds.), *Under the Sea: Archaeology and Palaeolandscapes of the Continental Shelf*. Coastal Research library (Vol. 20, pp. 335–359). Springer Int Publ. https://doi.org/10.1007/978-3-319-53160-1_22

Satow, C., Grant, K. M., Wulf, S., Schulz, H., Mallon, A., Matthews, I., & Lowe, J. (2020). Detection and characterisation of eemian marine tephra layers within the sapropel S5 sediments of the Aegean and Levantine Seas. *Quaternary*, *3*, 6. https://doi.org/10.3390/quat3010006

Satow, C., Tomlinson, E. L., Grant, K. M., Albert, P. G., Smith, V. C., Manning, C. J., et al. (2015). A new contribution to the Late Quaternary tephrostratigraphy of the Mediterranean: Aegean Sea core LC21. *Quaternary Science Reviews*, *117*, 96–112. https://doi.org/10.1016/j.quascirev.2015.04.005

Seymour, K. S., Christanis, K., Bouzinos, A., Papazisimou, S., Papatheodorou, G., Moran, E., & Dénès, G. (2004). Tephrostratigraphy and tephrochronology in the Philippi peat basin, Macedonia, Northern Hellas (Greece). *Quaternary International*, *121*, 53–65. https://doi.org/10.1016/j.quaint.2004.01.023

Seymour, K. S., & Vlassopoulos, D. (1989). The potential for future explosive volcanism associated with dome growth at Nisyros, Aegean volcanic arc, Greece. *Journal of Volcanology and Geothermal Research*, *37*, 351–364. https://doi.org/10.1016/0377-0273(89)90089-9

Shaw, B., & Jackson, J. (2010). Earthquake mechanisms and active tectonics of the Hellenic subduction zone. *Geophysical Journal International*, *181*, 966–984. https://doi.org/10.1111/j.1365-246x.2010.04551.x

Sigurdsson, H., Carey, S., Alexandri, M., Vougioukalakis, G., Croff, K., Roman, C., et al. (2006). Marine investigations of Greece's Santorini Volcanic Field. *Eos Trans AGU*, *87*(34), 337–342. https://doi.org/10.1029/2006EO340001

Simaiakis, S. M., Rijsdijk, K. F., Koene, E. F. M., Norder, S. J., Van Boxel, J. H., Sticchi, P., et al. (2017). Geographic changes in the Aegean Sea since the Last Glacial Maximum: Postulating biogeographic effects of sea-level rise on islands. *Palaeogeography, Palaeoclimatology, Palaeoecology*, *471*, 108–119. https://doi.org/10.1016/j.palaeo.2017.02.002

Simmons, J. M., Cas, R. A. F. F., Druitt, T. H., & Carey, R. J. (2017). The initiation and development of a caldera-forming Plinian eruption (172 ka Lower Pumice 2 eruption, Santorini, Greece). *Journal of Volcanology and Geothermal Research*, *341*, 332–350. https://doi.org/10.1016/j.jvolgeores.2017.05.034

Simmons, J. M., Cas, R. A. F. F., Druitt, T. H., & Folkes, C. B. (2016). Complex variations during a caldera-forming Plinian eruption, including precursor deposits, thick pumice fallout, co-ignimbrite breccias and climactic lag breccias: The 184 ka Lower Pumice 1 eruption sequence, Santorini, Greece. *Journal of Volcanology and Geothermal Research*, *324*, 200–219. https://doi.org/10.1016/j.jvolgeores.2016.05.013

Smith, P. E., York, D., Chen, Y., & Evensen, N. M. (1996). Single crystal 40Ar-39Ar dating of a Late Quaternary paroxysm on Kos, Greece: Concordance of terrestrial and marine ages. *Geophysical Research Letters*, *23*, 3037–3050. https://doi.org/10.1029/96gl02759

Sparks, R. S. J., & Wright, J. V. (1979). *Welded Air-Fall Tuffs* (Vol. 180, pp. 155–166). Geological Society of America Special Paper. https://doi.org/10.1130/spe180-p155

Stanley, D. J., & Sheng, H. (1986). Volcanic shards from Santorini (Upper Minoan ash) in the Nile Delta, Egypt. *Nature*, *320*, 733–735. https://doi.org/10.1038/320733a0

Stewart, A. L., & McPhie, J. (2006). Facies architecture and Late Pliocene – Pleistocene evolution of a felsic volcanic island, Milos, Greece. *Bulletin of Volcanology*, *68*, 703–726. https://doi.org/10.1007/s00445-005-0045-2

Sulpizio, R. (2005). Three empirical methods for the calculation of distal volume of tephra-fall deposits. *Journal of Volcanology and Geothermal Research*, *145*, 315–336. https://doi.org/10.1016/j.jvolgeores.2005.03.001

Tibaldi, A., Pasquare, F. A., Papanikolaou, D., & Nomikou, P. (2008). Discovery of a huge sector collapse at the Nisyros volcano, Greece, by on-land and offshore geological-structural data. *Journal of Volcanology and Geothermal Research*, *177*, 485–499. https://doi.org/10.1016/j.jvolgeores.2008.06.014

Tomlinson, E. L., Kinvig, H. S., Smith, V. C., Blundy, J. D., Gottsmann, J., Müller, W., & Menzies, M. A. (2012). The Upper and Lower Nisyros Pumices: Revisions to the Mediterranean tephrostratigraphic record based on micron-beam glass geochemistry. *Journal of Volcanology and Geothermal Research*, *243–244*, 69–80. https://doi.org/10.1016/j.jvolgeores.2012.07.004

Tomlinson, E. L., Smith, V. C., Albert, P. G., Aydar, E., Civetta, L., Cioni, R., et al. (2015). The major and trace element glass compositions of the productive Mediterranean volcanic sources: Tools for correlating distal tephra layers in and around Europe. *Quaternary Science Reviews*, *118*, 48–66. https://doi.org/10.1016/j.quascirev.2014.10.028

Vinci, A. (1985). Distribution and chemical composition of tephra layers from Eastern Mediterranean abyssal sediments. *Marine Geology*, *64*, 143–155. https://doi.org/10.1016/0025-3227(85)90165-3

Volentik, A., Vanderkluysen, & L., & Principe, C. (2002). Stratigraphy of the caldera walls of Nisyros volcano, Greece. *Eclogae Geologicae Helvetiae*, *95*, 223–235.

Waelbroeck, C., Labeyrie, L., Michel, E., Duplessy, J. C., McManus, J. F., Lambeck, K., et al. (2002). Sea-level and deep water temperature changes derived from benthic foraminifera isotopic records. *Quaternary Science Reviews*, *21*, 295–305. https://doi.org/10.1016/s0277-3791(01)00101-9

Wegwerth, A., Dellwig, O., Wulf, S., Plessen, B., Kleinhanns, I., Nowaczyk, N. R., et al. (2019). Major hydrological shifts in the Black Sea "Lake" in response to ice sheet collapses during MIS 6 (130–184 ka BP). *Quaternary Science Reviews*, *219*, 126–144. https://doi.org/10.1016/j.quascirev.2019.07.008

Wulf, S., Hardiman, M. J., Staff, R. A., Koutsodendris, A., Appelt, O., Blockley, S. P. E., et al. (2018). The marine isotope stage 1-5 cryptotephra record of Tenaghi Philippon, Greece: Towards a detailed tephrostratigraphic framework for the Eastern Mediterranean region. *Quaternary Science Reviews*, *186*, 236–262. https://doi.org/10.1016/j.quascirev.2018.03.011

Wulf, S., Keller, J., Paterne, M., Mingram, J., Lauterbach, S., Opitz, S., et al. (2012). The 100-133 ka record of Italian explosive volcanism and revised tephrochronology of Lago Grande di Monticchio. *Quaternary Science Reviews*, *58*, 104–123. https://doi.org/10.1016/j.quascirev.2012.10.020

Wulf, S., Keller, J., Satow, C., Gertisser, R., Kraml, M., Grant, K. M., et al. (2020). Advancing Santorini's tephrostratigraphy: New glass geochemical data and improved marine-terrestrial tephra correlations for the past ∼360 kyrs. *Earth-Science Reviews*, *200*, 102964. https://doi.org/10.1016/j.earscirev.2019.102964

Wulf, S., Kraml, M., Brauer, A., Keller, J., & Negendank, J. F. W. (2004). Tephrochronology of the 100 ka lacustrine sediment record of Lago Grande di Monticchio (southern Italy). *Quaternary International*, *122*, 7–30. https://doi.org/10.1016/j.quaint.2004.01.028

Wulf, S., Kraml, M., & Keller, J. (2008). Towards a detailed distal tephrostratigraphy in the Central Mediterranean: The last 20,000 yrs record of Lago Grande di Monticchio. *Journal of Volcanology and Geothermal Research*, *177*, 118–132. https://doi.org/10.1016/j.jvolgeores.2007.10.009

Wulf, S., Kraml, M., Kuhn, T., Schwarz, M., Inthorn, M., Keller, J., et al. (2002). Marine tephra from the Cape Riva eruption (22 ka) of Santorini in the Sea of Marmara. *Marine Geology*, *183*, 131–141. https://doi.org/10.1016/s0025-3227(01)00302-4

Zhao, Z., Mitchell, N. C., Quartau, R., Tempera, F., & Bricheno, L. (2019). Submarine platform development by erosion of a Surtseyan cone at Capelinhos, Faial Island, Azores. *Earth Surface Processes and Landforms*, *44*, 2982–3006. https://doi.org/10.1002/esp.4724

Zhou, X., Kuiper, K., Wijbrans, J., Boehm, K., & Vroon, P. (2021). Eruptive history and $^{40}Ar/^{39}Ar$ geochronology of the Milos volcanic field, Greece. *Geochronology*, *3*, 273–297. https://doi.org/10.5194/gchron-3-273-2021

Zhu, L., Mitchell, B. J., Akyol, N., Cemen, I., & Kekovali, K. (2006). Crustal thickness variations in the Aegean region and implications for the extension of continental crust. *Journal of Geophysical Research*, *111*, B01301. https://doi.org/10.1029/2005JB003770